Cite this article as: Emmrich S., et al. (2024). Characterization of Naked Mole-Rat Mesenchymal Stromal Cells: Comparison with Long- and Short-Lived Mammals, *AgingBio*, *2*, e20240029. doi: 10.59368/agingbio.20240029.

Research Paper

Characterization of Naked Mole-Rat Mesenchymal Stromal Cells: Comparison with Long- and Short-Lived Mammals

Stephan Emmrich,[1] Alexandre Trapp,[1] Adit Ganguly,[1] Ali S. Biashad,[1] Yulia Ablaeva,[1] Michael G. Drage,[2] Masaki Takasugi,[1] Andrei Seluanov,[1,*] and Vera Gorbunova[1,*]

[1]Departments of Biology and Medicine, University of Rochester, Rochester, NY, USA

[2]Department of Pathology and Laboratory Medicine, University of Rochester Medical Center, Rochester, NY, USA

[*]Corresponding authors: andrei.seluanov@rochester.edu; vera.gorbunova@rochester.edu

Stephan Emmrich and Alexandre Trapp have equally contributed to this research.

https://doi.org/10.59368/agingbio.20240029

Received: 3/11/2024, Revised: 5/16/2024, Accepted: 5/22/2024, Published: 6/28/2024

Mesenchymal stem and stromal cells (MSCs) show therapeutic potential by facilitating tissue repair. Here, we describe the isolation and initial characterization of MSCs from the longest-lived rodent, the naked mole rat (NMR). NMR MSCs display the *CD90/THY1* surface marker characteristic of human and mouse MSCs. The tri-lineage differentiation capacity of NMR MSCs revealed a bias toward osteogenic differentiation and limited adipogenic potential. Upon passaging in culture, NMR MSCs enter a senescence-like state characterized by growth arrest, senescent morphology, diminished *CD90/THY1*, and activated tumor suppressive signaling. The presence of a senescence-like state makes NMR MSCs more similar to human MSCs than to mouse MSCs. However, unlike human MSCs that do not spontaneously immortalize, NMR MSCs eventually give rise to immortalized, rapidly proliferating clones. Unique gene expression profiles of NMR MSCs compared to human and mouse counterparts showed the absence of *CXCL12* production, low levels of DNA methylases, and high levels of Sirtuins 1/2/3/6, raising intriguing questions about their contributions to the NMR's remarkable longevity. In summary, our study identified unique features of NMR MSCs, offering insights into a potentially therapeutically relevant stem cell population in a long-lived species. Further studies are crucial to uncover the underlying molecular mechanisms and their implications for human health and aging.

Introduction

The naked mole rat (NMR), *Heterocephalus glaber*, a mouse-sized rodent, is a unique model for aging research due to its exceptional longevity and resistance to age-related diseases[1]. The maximum lifespan of NMRs exceeds 40 y in captivity, which, combined with a minimal age-related decline in physiological functions, makes this animal a treasure trove for the discovery of natural anti-aging mechanisms[2,3]. Various factors converge in shaping the NMR's extraordinary health and longevity; these include enhanced proteostasis, robust antioxidant defenses, translational fidelity, and potent tumor suppressor pathways, including high molecular weight hyaluronan (HMW-HA) secretion and a unique *INK4/ARF* locus splicing product[4–8].

Mesenchymal stem cells (MSCs) represent a subset of adult stem cells residing in various niches, including bone marrow (BM), adipose tissue, and umbilical cord tissue. They are characterized by their remarkable capacity for self-renewal and differentiation into multiple cell lineages, including osteoblasts, chondrocytes, adipocytes, and even non-mesodermal cell types, such as neurons[9]. This pluripotent nature endows MSCs with the ability to contribute to tissue regeneration and repair processes, making them pivotal players in maintaining tissue homeostasis and integrity. While the terms "mesenchymal stem cells" and "mesenchymal stromal cells" have historically been used interchangeably, a growing consensus recognizes their distinct properties. Both cell types share common surface markers and characteristics, such as fibroblast-like morphology and immunomodulatory potential. However, the differentiation potential sets them apart[10]. MSCs demonstrate robust multipotency and can give rise to mature cell lineages, whereas MSCs are believed to possess a broader immunomodulatory role, influencing immune responses through paracrine signaling[11]. MSC-derived soluble factors were shown to suppress immune cell activation and promote immune tolerance[12]. This immunomodulatory ability has been harnessed in transplantation medicine to mitigate graft-versus-host disease and improve graft acceptance[13].

As aging progresses, the regenerative potential of MSCs diminishes, attributed in part to epigenetic changes and senescence-associated alterations[14]. These age-related shifts impact the regenerative capacity of tissues, contributing to the increased susceptibility to age-related diseases. Beyond their diminished regenerative capabilities, MSCs participate in the intricate interplay between stem cell niche dysfunction and aging-related pathologies. Secreted factors from senescent MSCs, termed the senescence-associated secretory phenotype (SASP), have been implicated in promoting inflammation and tissue damage, a

phenomenon linked to age-related disorders[15]. Addressing the age-related alterations in MSC function holds potential for mitigating the effects of aging on tissue integrity and systemic health.

Here, we isolated and characterized primary MSCs from NMRs by in vitro cultivation, differentiation, and bulk RNA sequencing (RNA-Seq). We found distinct gene expression in NMR MSCs compared to human and mouse counterparts, marked by high levels of Sirtuins expression and low levels of expression of the DNA methylation machinery. NMR MSCs were *CD90/THY1* positive, differentiated in vitro toward the osteogenic lineage, and, upon prolonged cultivation, underwent premature senescence and lost differentiation potential.

Methods

Animal and human samples

ll animal experiments were approved and performed in accordance with guidelines instructed by the University of Rochester Committee on Animal Resources. NMRs were from the University of Rochester colonies, with housing conditions as described[16]. Wild-type C57BL/6 mice were obtained from JAX. Human bone spicules were obtained from amputated bone at University of Rochester Medical Center (URMC), courtesy of Dr. Michael Drage.

Cell isolation and culture

MSCs were obtained by isolating bones from animals and placing them in α-MEM (Minimum Essential Medium Eagle Alpha Modification, with ribonucleosides, deoxyribonucleosides and sodium bicarbonate, without L-glutamine) on ice until they could be processed in a sterile hood. Hematopoietic cells were removed by flushing the marrow in the bone cavity with a 0.45-mm syringe needle. Bones were crushed and digested with collagenase as described[17]. Digested bones were plated in MSC expansion medium: α-MEM (Sigma), 10% MSC-qualified FBS (Gibco), 1% GlutaMax (Gibco), and 1% Pen-Strep (Gibco). 1x Antibiotic/Antimycotic (Gibco) was added to bone cultures for up to one week to prevent contamination. Adherent cells were dissociated with warm 0.25% Trypsin/EDTA for the minimum amount of time required in order to preserve cell viability and surface marker expression. Bone fragments were reseeded on new plates to enable more cells to sprout from the bones and were eventually discarded. Adherent cells were cultured separately and passaged when reaching 70%–80% confluence. Media changes were conducted every three days. Skin fibroblast (SF) cells were isolated from mouse and NMR as described[18]. SFs were grown in E-MEM with L-glutamine (ATCC), 15% FBS (Gibco), and 1% Pen-Strep. NMR cells were grown at 32°C at 5% CO_2 and 3% O_2, while mouse and human cells were grown at 37°C at 5% CO_2 and 3% O_2. Upon trypsinization, cells were centrifuged at 400*g* for 5 min and resuspended in MSC expansion medium. Cells were then counted manually using a hemocytometer. Cells were cryopreserved in FBS (Gibco) + 10% DMSO (Fisher) at −80°C, followed by transfer to liquid nitrogen storage. Images of cells were captured at 40× magnification on a Nikon TS100 inverted phase contrast microscope.

Population doubling (PD) analysis

Using the number of cells seeded on a plate (S) and the number of cells harvested at the end of a given culture period (H), it was possible to calculate PD levels (PDLs) and cumulative PD (CPD) with the following formulas[19]:

$$\mathrm{PDL} = \frac{(\log_{10}\mathrm{H} - \log_{10}\mathrm{S})}{\log_{10}2} \quad (1)$$

$$\mathrm{CPD}_n = \mathrm{CPD}_{n-1} + \mathrm{PDL} \quad (2)$$

Since hematopoietic contamination can misrepresent adherent cell count when cells are dissociated from bone plates, PDL, CPD, and "days in culture" calculations were started at P1.

Flow cytometry

Flow cytometry analysis and cell sorting were conducted at the URMC Flow Core. Cells to be assayed were resuspended in FACS Buffer, composed of 1x PBS (Gibco), 2% FBS (Gibco), and 2-mM EDTA (Invitrogen), and kept on ice. Cells were stained with the following antibodies for 15 min at room temperature in the dark (to prevent loss of fluorescence activity): CD90.1/Thy1.1_PECy7 (OX-7), CD34_APC (581), CD90.2_PECy7 (53-2.1), Sca-1_APCCy7 (D7), CD146_APC (ME-9F1), mouse lineage cocktail FITC (145-2C11, RB6-8C5, RA3-6B2, Ter-119, M1/70), all Biolegend; CD166/ALCAM_PE (eBioALC48), Invitrogen. Cells were washed with FACS Buffer after staining, centrifuged at 400*g* for 5 min, and resuspended in FACS Buffer containing 10-nM SYTOXGreen viability dye (Invitrogen). Stained and unstained samples were kept on ice until analysis of Flow Cytometers (BD). For C12FDG staining, we followed the protocol as described[20].

Neonate MSC proliferation and marker expression assays

Neonate MSCs from frozen P2 aliquots were thawed on 15-cm culture dishes and harvested upon reaching 80%–90% confluence. Cells were stained with PE-Cy7-conjugated CD90.1/Thy1.1 antibody and SYTOX Green and sorted based on CD90 expression. A buffer zone was included in the sorting workflow to only select for highly positive and highly negative cells. Sorted positive and negative cells were seeded on uncoated plates. Cells were counted during harvest, and 200,000 cells were replated. The remaining cell populations were analyzed for CD90.1 marker expression via flow cytometry.

Osteogenic differentiation assays

To assess the osteogenic differentiation capacity of the MSCs, cells were seeded at a density of 10,000/well in a six-well plate format and cultured in osteogenic induction medium (OIM) or control expansion medium. OIM was composed of expansion medium supplemented with 0.1-μM Dexamethasone (Sigma), 50-μM L-Ascorbic acid 2-phosphate (Sigma), and 10-mM β-Glycerol phosphate (Sigma). The media was changed at three-day intervals. In certain assays, OIM was additionally supplemented with 2-μM purmorphamine (PMN), and DMSO was used to control for the effect of the vehicle in control wells. Alkaline phosphatase (AP) staining was conducted after 2 weeks in culture using the Leukocyte Alkaline Phosphatase Kit (cat no. 86C, Sigma). Following the manufacturer's protocol, cells were fixed using Citrate-Acetone-Formaldehyde Fixative for 30 sec. Cells were stained with a mixture of FBB-alkaline solution, sodium nitrite, naphthol AS-BI alkaline solution, and distilled water for 15 min in the dark. Von Kossa staining was conducted after 4 weeks in culture, following a modification of the protocol outlined in (Zhu et al., 2010). Cells were fixed in 10% formalin for 20 min, washed with distilled water, and then stained with a 5%

(wt/vol) silver nitrate water solution under UV light for 30 min. Cells were washed three times with distilled water, then immersed in a 5% (wt/vol) sodium thiosulfate solution of water for 5 min. Cells from both assays were ultimately washed with distilled water, and plates were scanned.

Adipogenic differentiation assays

To assess the adipogenic differentiation capacity of the MSCs, cells were seeded at a density of 10,000/well in a six-well plate format and cultured in adipogenic induction medium (AIM) or control expansion medium. AIM was composed of expansion medium supplemented with 1-μM Dexamethasone (Sigma), 500-μM 3-isobutyl-1-methylxanthine (Sigma), and 10 μg/mL human recombinant insulin (Sigma). AIM was further supplemented with 1-μM Rosiglitazone (Cayman Chemical), 40-μM Indomethacin (Sigma), or a combination of both compounds. DMSO was added to the control wells to standardize the deleterious effect of the vehicle. The media was changed at three-day intervals. Adipogenesis was assayed at 2, 3, and 4 weeks using the Oil Red O stain. Oil Red O powder (Sigma) was dissolved at a concentration of 0.5% (wt/vol) in pure isopropanol and allowed to stand for 5 min. Some of the solution was carefully transferred to a new tube, making sure to avoid transferring undissolved Oil Red O powder that had accumulated at the bottom. The transferred solution was then diluted to 60% isopropanol with distilled water, properly mixed, and allowed to stand for 5 min. The solution was then filtered through a 0.2-μM polyethersulfone syringe filter. Cells were fixed in 10% formalin for 20 min, rinsed with PBS, and allowed to dry completely. Cells were then stained for 15 min with the filtered 60% Oil Red O solution. The wells were then washed with distilled water and scanned. High-resolution images were captured using a Nikon Eclipse Ti inverted microscope.

Chondrogenic differentiation assays

To assess the chondrogenic differentiation of MSCs, cells were harvested and transferred to polypropylene tubes to prevent cell adhesion to the plastic. Cells were centrifuged at 400*g* for 5 min and resuspended in chondrogenic induction medium (CIM) or control medium. CIM was composed of high-glucose D-MEM with GlutaMax (Gibco), 0.1-μM Dexamethasone (Sigma), 1% (vol/vol) Insulin-Transferrin-Selenium (Sigma), 1% Pen/Strep (Gibco), 50-μM ascorbate-2-phosphate (Sigma), 1-mM sodium pyruvate (Gibco), 50-μg/mL L-proline (Sigma), and 20-ng/ml TGF-β3 (R&D Systems). The control medium was composed of D-MEM with GlutaMax, 1% Pen/Strep, and 10% MSC-qualified FBS (Gibco). Cells were cultured vertically in polypropylene tubes for 3 weeks, with media changes every 3 days. Conditioned media was manually aspirated with a pipettor to prevent inadvertent loss of the cell pellet. Upon termination of the culture period, pellets were centrifuged at 300*g* for 5 min, and medium was removed and replaced with 10% formalin. Pellets were stored at room temperature until they could be processed. Pellets were subsequently embedded in paraffin, sectioned, stained (either with Hematoxylin/Eosin or Alcian Blue Hematoxylin/Orange G), and imaged by Dr. Michael Drage.

Hedgehog cell viability assays

To test the effect of the functionally opposite hedgehog interfering compounds cyclopamine and PMN, cells were seeded at a density of 5,000/well in a 96-well plate format. Only the inner 32 wells were utilized (8 concentrations, 4 technical replicates each), and the remaining wells were filled with PBS to minimize edge effects. Cells were cultured in their respective expansion medium (supplemented α-MEM or E-MEM for MSCs and fibroblasts, respectively) containing varying concentrations of PMN/cyclopamine, ranging from 0 to 33.3 μM. The DMSO concentration was equalized in all wells to compensate for the exclusive solubility of these compounds in DMSO and its necessary usage as a vehicle. Cells were cultured for 6 days, with a half-medium change to prevent disrupting the cell monolayer on day 3. Cell viability was assayed on day 6 with CellTiter-Glo2.0 (CTG, Promega). 40 μL of CTG were added directly to the medium, and plates were placed on an orbital shaker for 5 min to allow proper mixing and cell lysis. Luminescence was allowed to stabilize for 10 min prior to measurement and was subsequently measured with no lid using a Tecan plate reader with an integration time of 1 sec/well. Once the minimal effective concentrations of both compounds were determined, MSCs were seeded on six-well plates at a density of 150,000/well. Cells were grown in DMSO-controlled MSC expansion medium or MSC expansion supplemented with either 1-μM PMN or 10-μM cyclopamine. Cells were harvested at 24-hour intervals beginning on days 2 and 3 for cyclopamine and PMN, respectively. Cells were stained with Annexin V conjugated to APC/Fire 750 (BioLegend) in Annexin binding buffer, washed, and subsequently stained with 4',6-diamidino-2-phenylindole (DAPI) as a viability stain. Proportions of cells in the three distinct states (viable, apoptotic, and dead) were quantified using Kaluza software (Beckman Coulter).

Seahorse metabolic function assay

To assess oxygen consumption rate (OCR) and extracellular acidification rate (ECAR), cells were seeded at a density of 25,000/well in 80 μL on Seahorse XF96 tissue culture microplates (Agilent). Since so many cell samples needed to be seeded on the same plate, cells were trypsinized in batches of three and subsequently seeded on the plates, each in three technical replicates. Following each batch, the XF96 microplate was centrifuged at 300*g* for 1 min with the lowest centrifugal deceleration setting to ensure that all cells were evenly distributed on the flat surface at the bottom of the plate and not on the sides of the well. Cells were incubated in their respective mediums for 24 hours at 32°C. The next day, cells were washed following the manufacturer's protocol. A multichannel pipette was used to remove 55 μL of medium, and wells were washed twice with 200 μL of RPMI assay medium. A final assay volume of 180 μL/well was used. Cells were incubated for 60 min at 37°C in the absence of CO_2 and measured using the Seahorse XFe96 Analyzer (Agilent) at the URMC Flow Core.

Quantitative PCR (qPCR)

NMR-sorted MSCs of different passage numbers were used for RNA extraction by Trizol (Thermo Fisher). RNA was quantified using a NanoDrop One (Thermo Fisher), and 100 ng was used as input for the High Capacity cDNA Reverse Transcription Kit (Thermo Fisher). The RT reaction was performed according to instructions, and the 20 μl reaction was diluted to 200 μl, of which 5 μl were used per qPCR reaction. We used iTaq Universal SYBR Green Supermix (Bio-Rad) on a CFX Connect® RealTime System (Bio-Rad) with a three-step cycling of 10 sec 95°C, 20 sec 60°C, and 30 sec 72°C for 40 cycles. All primers (IDTDNA) were validated to amplify a single amplicon at the above PCR conditions by gel electrophoresis. Gene sequences for primer design by Primer3Plus were retrieved from ENSEMBL.

Bulk RNA-Seq

RNA from cultured mouse, human, and NMR MSCs was paired-end sequenced at ~100 million reads and 150 bp fragment length on a NovaSeq 6000 (Illumina). We used the TruSeq® Stranded mRNALibrary Prep (Illumina) for library preparation. RNA-Seq datasets for mouse and NMR fibroblast populations were taken from Zhao et al. and processed from raw fastq files[21]. Raw Illumina paired-end sequencing reads were subjected to base-quality trimming using Trimmomatic and assessed with FastQC[22]. Salmon v1.10.1 was used to calculate expected counts and transcripts per million (TPMs)[23], using the NMR transcriptome reference from Lu et al., while mouse and human transcriptome references were obtained from Ensembl 104 assembly[24].

Subsequent analysis was done with *>= R 4.2.1* and *Bioconductor*. For intra-species NMR MSC comparisons (**Fig. 6**), expected counts from different transcript isoforms of the same gene were added up to one unique identifier (uniquify) using the `ddply` and `numcolwise` functions of the *plyr* package, while *edgeR* was used to calculate size factors with `method = "Relative Log Expression"` and to compute counts per million (CPMs). We applied *genefilter* to calculate the interquartile range (IQR) of CPMs with `IQR(x) > 1` to filter unexpressed and outlier genes; library-size normalized, IQR-filtered log2-transformed CPMs were vst-transformed by *DESeq2*, then a PCA embedding from the stats package was used as input for *Rtsne*. We applied *limma* to perform voom-transformation and select for differentially expressed genes (DEGs) with $p < 0.05$ and log-fold change 1. The *fGSEA* package was used to retrieve leading edge genes after performing gene set enrichment analysis (GSEA) under default conditions[25], with the required rank metric generated after Plaisier et al.[26].

For the interspecies comparison, human, mouse, and NMR TPM datasets (**Fig. 1**) were joined based on HGNC symbols (a.k.a., gene name), which are shown in **Figure S1A** as detected transcripts with ortholog IDs for each species. We uniquified these transcripts to genes as for intra-species comparisons above, then used the gene name as a common ortholog identifier to match and merge TPM datasets between species. The Euler–Venn diagram in **Figure S2A** shows 10,430 common gene names across three species, along with partial and unmatched gene names. The next *genefilter* was used to calculate the IQR of TPMs with `IQR(x) > 1` to filter unexpressed and outlier genes. The *TCC* package was used to calculate TMM-based size factors. The function `betweenLaneNormalization` with median scaling from the *EDASeq* package was used to normalize for sequencing batch effects. DGE and GSEA were performed as above, using the species as a contrast and the MsigDB v6.0 hallmark gene sets.

Quantification and statistical analysis

Data are presented as the mean ± standard deviation (SD). Statistical tests performed can be found in the figure legends. P values of less than 0.05 were considered statistically significant. Statistical analyses were carried out using Prism 9 software (GraphPad) unless otherwise stated.

Results

MSC cultures of short- and long-lived mammals

To characterize NMR MSCs and investigate whether they have any distinguishing features that may contribute to NMR longevity, we set out to isolate MSCs from NMRs. For comparison, we isolated MSCs from BM of three other long-lived species: *Homo sapiens* (healthy donors), *Eptesicus fuscus* (big brown bat), *Spalax galili* (blind mole rat [BMR]), and three short-lived rodent species: *Mus musculus* (C57BL6 laboratory mouse strain), *Rattus norvegicus* (Fisher and Lewis laboratory strains), and *Fukomys damarensis* (Damaraland mole rat [DMR]). DMRs are eusocial African mole rats that are phylogenetically close to NMRs and display a threefold shorter lifespan.

Mouse, rat, and bat cells showed the fastest outgrowth of MSCs from bone shards in culture dishes, with initial colony-forming cell clusters appearing as early as days 3–5 (**Fig. 1B**). Interestingly, both DMR and BMR cells formed distinguishable cell clusters at days 5–7; human MSCs formed clusters at days 7–14, whereas NMR MSCs took longer than 21 days to form bone shard-derived cell outgrowth. These patterns are largely correlated with the proliferation rates observed for each species as discussed below and may reflect both cell-intrinsic growth suppressive signaling as well as adaptation to culture conditions.

We measured the PD for at least 30 days in all species, and some specimens were cultured longer than 180 days (**Fig. 1A**). Rat and mouse MSCs displayed rapid logarithmic growth for over 48 days of culture, with rat cells growing faster. Mouse MSCs were cultured continuously for 155 days and displayed a constant logarithmic growth pattern. Bat MSCs displayed the highest proliferation rate. Human MSC growth was consistent with previous reports[27], with initial logarithmic growth followed by growth arrest. Human MSC proliferation declined steadily up PD 22 ± 1.5, when a plateau was reached at 98 ± 2 days of culture. The difference in PD numbers achieved was likely due to the differences in media composition. Schellenberg et al. used 10% human platelet lysate in DMEM with low glucose, effectively supporting human MSC in vitro culture, whereas in our study we used a single formulation with 10% FBS in αMEM to facilitate crossspecies comparison. In these conditions, DMR and BMR MSCs showed a higher growth rate than human MSCs until PD 10 ± 1 (**Fig. 1A**). DMR cells reached plateau at 70 ± 4 days with a PD of 25 ± 5. BMR MSCs plateaued their proliferation at 101 ± 4 days with PD 24 ± 3, and in three of the four tested specimens, the in vitro growth arrest was maintained up to 280 days in culture (**Fig. 1A**). However, the remaining one BMR MSC culture continued to proliferation as a spontaneously immortalized line. NMR MSCs entered obligate growth arrest at 30 ± 2 days in culture with PD 8.5 ± 0.8. Interestingly, all six NMR MSC lines re-emerged from this temporary cell cycle arrest at 90 ± 5 days of culture and continued in vitro proliferation as spontaneously immortalized cells. Thus, while NMR cells grew slower and exhausted earlier than MSCs of all other long-lived species, they re-entered cell cycling around the time window of culture when DMR, BMR, and human MSC proliferation plateaued. This result suggests that NMR MSCs undergo growth arrest when cultured in vitro, which may correspond to tumor suppressive senescence. While BMR cells display a sustained cell cycle arrest, in NMRs, immortalized clones emerge.

In summary, we established the in vitro PD kinetics of BM-derived MSCs across seven species. We observed distinct growth patterns where mouse, rat, and bat MSCs proliferate continuously, while human, BMR, DMR, and NMR cells undergo growth arrest, with NMR cultures undergoing spontaneous immortalization after ~100 days in culture.

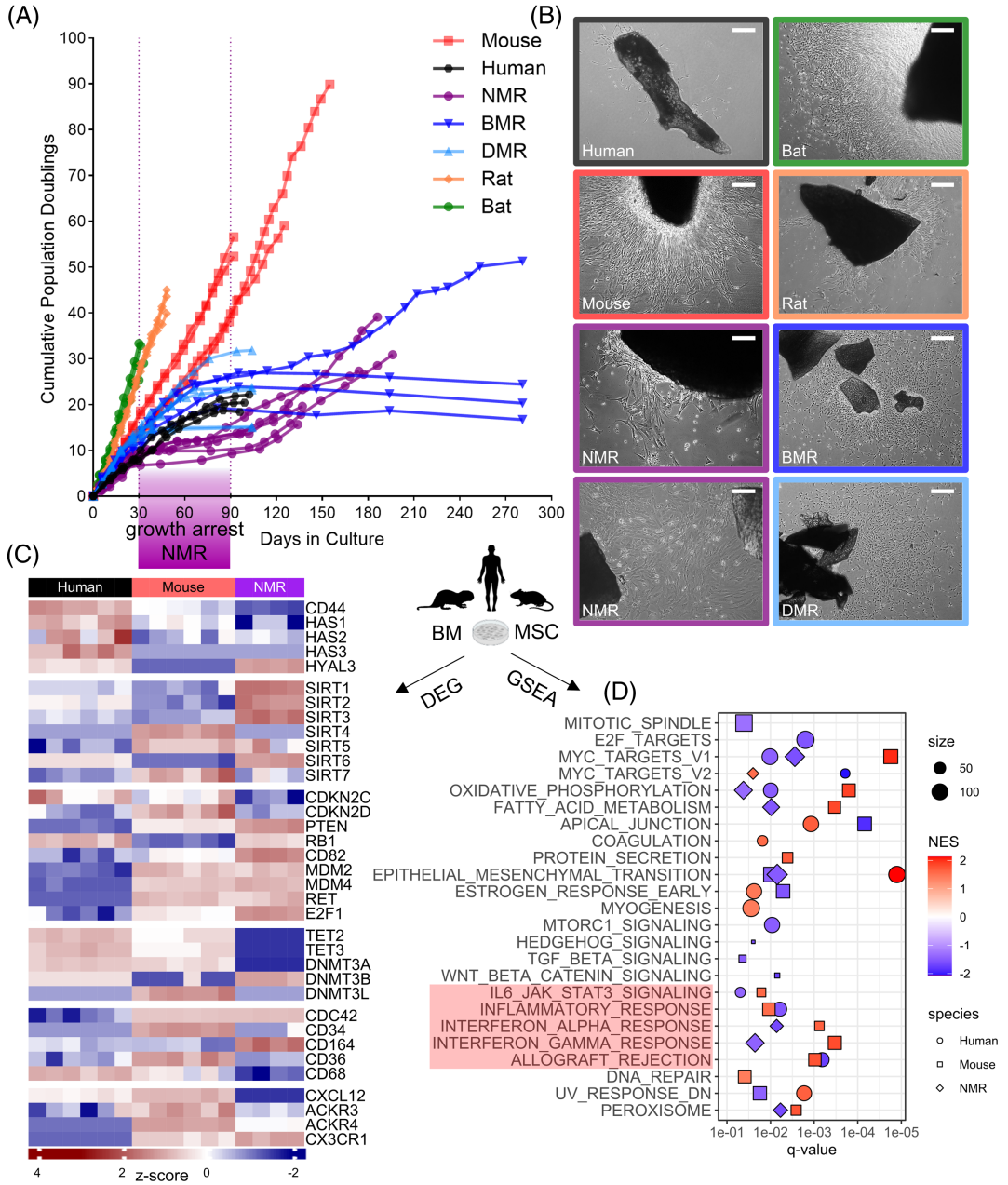

Figure 1. Naked mole-rat (NMR) mesenchymal stem cells (MSCs) show distinct in vitro proliferation and gene expression patterns. (A) Population doublings (PDs) curve of primary MSC cultures from indicated species; highlighted in purple is the average temporary growth arrest period of NMR MSCs. **(B)** Representative micrographs of clonal MSC outgrowth from bone tissue shards for each species; image border colors for species reference are the same as in panel (A). NMR, 20× objective scale bars 200 μm; all other species, 10× objective with scale bars 100 μm. **(C)** Selected ortholog expression across species from voom-transformed, z-score-centered transcripts per million. **(D)** Fast preranked gene set enrichment analysis (GSEA) across common orthologs between the three species using the MSigDb hallmark gene set collection; $q < 0.05$. See also **Figure S1** and **Tables S1 and S2**.

Comparison of expression patterns between human, mouse, and NMR MSCs

To perform molecular characterization of NMR MSCs, we compared the transcriptomes of NMR, human, and mouse MSCs. Since MSC isolates are known to accumulate DNA damage and other molecular lesions over an extended culture period[28,29], we collected the first cell clusters growing from primary bone shard material in culture dishes before the first passage as input material for crossspecies bulk RNA-Seq comparisons. RNAseq reads obtained from fresh MSC cultures from human, mouse, or NMR BM were each aligned to their respective transcriptome references. Human samples had the highest, while NMR samples had the lowest numbers of total detected transcripts and transcripts with gene symbol ortholog IDs (**Fig. S1A**). When transcripts were subsumed to genes for crossspecies ortholog-based ID matching, a total of 10,430 genes were conserved between three references (**Fig. S1B**). Using this ortholog intersection, we integrated and normalized six humans and six mice with four NMR MSC biological replicates (**Fig. S1C**). Multidimensional scaling clearly separated the species, with 87% loadings in the

first two dimensionalities (**Fig. S1D**). Hierarchical clustering yielded DEG groups specifically up- and downregulated for each species relative to the other two species (**Fig. S1E,F**). We found 1,184 up- and 779 downregulated genes for human MSCs, 780 up- and 1,125 downregulated murine genes, and 1,034 up- and 1,420 downregulated NMR-specific genes.

Remarkably, NMR MSCs upregulated multiple sirtuin family members *SIRT1/2/3* and especially the longevity-associated SIRT6[30,31], implicated in cellular stress resistance, genomic stability, aging, and energy homeostasis. Surprisingly, hyaluronic acid (HA) receptor *CD44*, which is associated with longevity[32], as well as HA synthase genes *HAS1*, *HAS2*, and *HAS3*, which evolved to produce high molecular mass HA in subterranean species[33], were downregulated in NMR MSCs (**Fig. 1C**). The only hyaluronidase present in all three references, *HYAL3*, was upregulated in NMR MSCs. As HMW-HA suppresses malignant transformation in NMR fibroblasts[8], reduced expression of hyaluronan synthases and increased expression of the hyaluronan degrading gene in NMR MSCs may contribute to the ease of immortalization displayed by these cells (**Fig. 1A**).

The expression landscape of tumor-promoting and antagonizing factors conveyed a mixed impression: *ATF1* triggering cell proliferation and transformation, proto-oncogenic *KRAS*, and growth-promoting *MKI67* and *FGF7*, along with crucial players of the Hippo signaling pathway *STK3*, *YAP1*, and *YES1*, were specifically downregulated in NMR MSCs (**Fig. S1F**). However, NMR MSCs overexpressed *VGF* and the nutrient-insensitive *mTORC2* complex subunit *RICTOR*, whereas *RAD51B* and *RAD51D* mediating the homologous recombination repair pathway of double-stranded DNA breaks were strongly silenced in NMR MSCs, which may reflect a slower proliferation rate (**Fig. S1E,F**). Moreover, while NMR MSCs expressed *RB1* at levels similar to human MSCs and showed the highest expression of tumor suppressors *PTEN* and *CD82*, they overexpressed the p53 inhibitors *MDM2/4*, the proto-oncogene *RET*, and *E2F1*, and showed very low levels of p18-*INK4C* as well as p19-*INK4D*, which control G_1 cell cycle progression (**Fig. 1C**). In addition, the central effectors of the DNA methylation machinery involving *TET2/3* and *DNMT3A* were absent, *DNMT3L* was underexpressed, and only *DNMT3B* was detected in NMR MSCs, potentially pointing toward global hypomethylation.

MSCs are an integral part of the hematopoietic niche and are required for stem cell maintenance and proper blood formation. While the role as a critical niche factor is likely conserved, with regard to hematopoietic marker gene expression, species-specific patterns emerged, such as similar levels of the stem cell polarity master regulator *CDC42* in rodents but very low expression in human MSCs (**Fig. 1C**)[34]. Likewise, *CD34* is an exclusion marker for human MSCs, not expressed in NMR MSCs, and in both species the prospective marker for isolation of the primitive hematopoietic stem and progenitor cell (HSPC) pool[35–37]. Moreover, NMR MSCs highly expressed *CD164*, an adhesion molecule for HSPCs[38], which has recently been shown to functionally enrich human *CD34+* HSPCs into long-term repopulating stem cells[39]. Interestingly, the scavenger receptor *CD68*, highly expressed on monocytes, macrophages, and fibroblasts[40], which we confirmed to be expressed in human MSCs[41], was absent in NMR MSCs. By interacting with HSPCs, MSCs have been implicated in the production and secretion of SDF-1a (*CXCL12*), the major hematopoietic stem cell homing cytokine[42]. Remarkably, while *CXCL12* is moderately expressed in human MSCs and overexpressed in mouse MSC, it is absent in NMR MSCs. Furthermore, alternative chemokine receptors *ACKR3/4* are expressed at very low levels in both human and NMR MSCs, of which *ACKR3* (*CXCR7*) acts as a receptor of *CXCL12*, activating the *MAPK* signaling pathway[43–45]. However, NMR MSCs upregulated *CX3CR1*, the fractalkine receptor present on many early leukocytes and involved in inflammation, adhesion and chemotaxis[46]. These transcriptional programs suggest altered dynamics of homeostasis and functional cross talk between cellular components of the hematopoietic niche in NMRs.

To examine the pathways pertaining to species-specific gene expression programs, we performed GSEA on MSigDb hallmark pathways (**Fig. 1D**). Multiple gene sets related to inflammation were enriched in mouse cells, as we described earlier in three-way crossspecies comparisons of hematopoietic systems[26,36]. On the gene level, mouse MSCs overexpressed *SLPI*, *CSF2RA*, *CSF1*, *FAS*, *TLR2*, *IL15/IL15RA*, and *IL1RL2*, whereas human MSCs downregulated *APOE*, *IFNAR2*, and *IRAK2*, and similarly, NMR MSCs showed very low levels of *IL6* and *CCL5* (**Fig. S1E,F**). Although NMR MSCs overexpressed five collagen variants, human MSCs strongly enriched for epithelial-to-mesenchymal transition and apical junction pathways, exemplified by overexpression of extracellular matrix (ECM) components elastin, fibronectin 1, several collagen homologs, and others (**Fig. S1E,F**; **Table S2**), whereas mouse MSCs downregulated tubulin and had consistently higher expression of *CDC42* compared to human MSCs (**Fig. 1C**). The single positively enriched hallmark pathway for NMR MSCs was Myc targets V2, scored through leading edge genes such as *RCL1*, *PRMT3*, *NPM1*, and *PLK1*.

Taken together, gene expression programs markedly differed across species, with the predominant distinguishable feature being upregulation of inflammatory pathways in mouse MSCs compared to NMR and human.

NMR MSCs and fibroblasts show distinct proliferation and gene expression patterns

Fibroblasts are stromal cells that share morphological and molecular markers with MSCs, which in turn have the capacity to differentiate into fibroblasts[47]. Recent evidence suggests that both cell types are ubiquitous stromal elements in the same tissues and show immunomodulatory and regenerative properties[48,49]. Here, we compared cultured mouse (MSF) and NMR skin fibroblasts (NSF) with BM MSCs and report that all four cell types can be readily distinguished from each other. Brightfield microscopy of cultured cells did not reveal morphological differences between fibroblasts and MSCs; however, NSFs showed clear early contact inhibition (ECI; **Fig. 2A**), a cancer resistance mechanism mediated by the secretion of HMW-HA and the maintenance of checkpoint inhibitor activity[50,51]. The ECI phenotype has been observed in fibroblasts from diverse NMR tissues, and its absence in MSCs is an indicator of a separate cell population from NMR BM. While the growth kinetics of MSFs and MSCs were essentially identical, NSFs proliferate slower than NMR MSCs but do not enter the growth arrest phase (**Fig. 2B**). Interestingly, an NSF clone which spontaneously lost ECI upon prolonged culture showed a marked increase in the rate of proliferation.

Due to the important role of HMW-HA in tumor suppression in the NMR, we quantified the amount of HA in the supernatants of cultured mouse and NMR cells using gel electrophoresis as described previously[52]. Confirming earlier reports, NSF secreted abundant HMW-HA >15 kDa (**Fig. S2A**). NMR MSCs of low or high passage secreted abundant HA of lower molecular

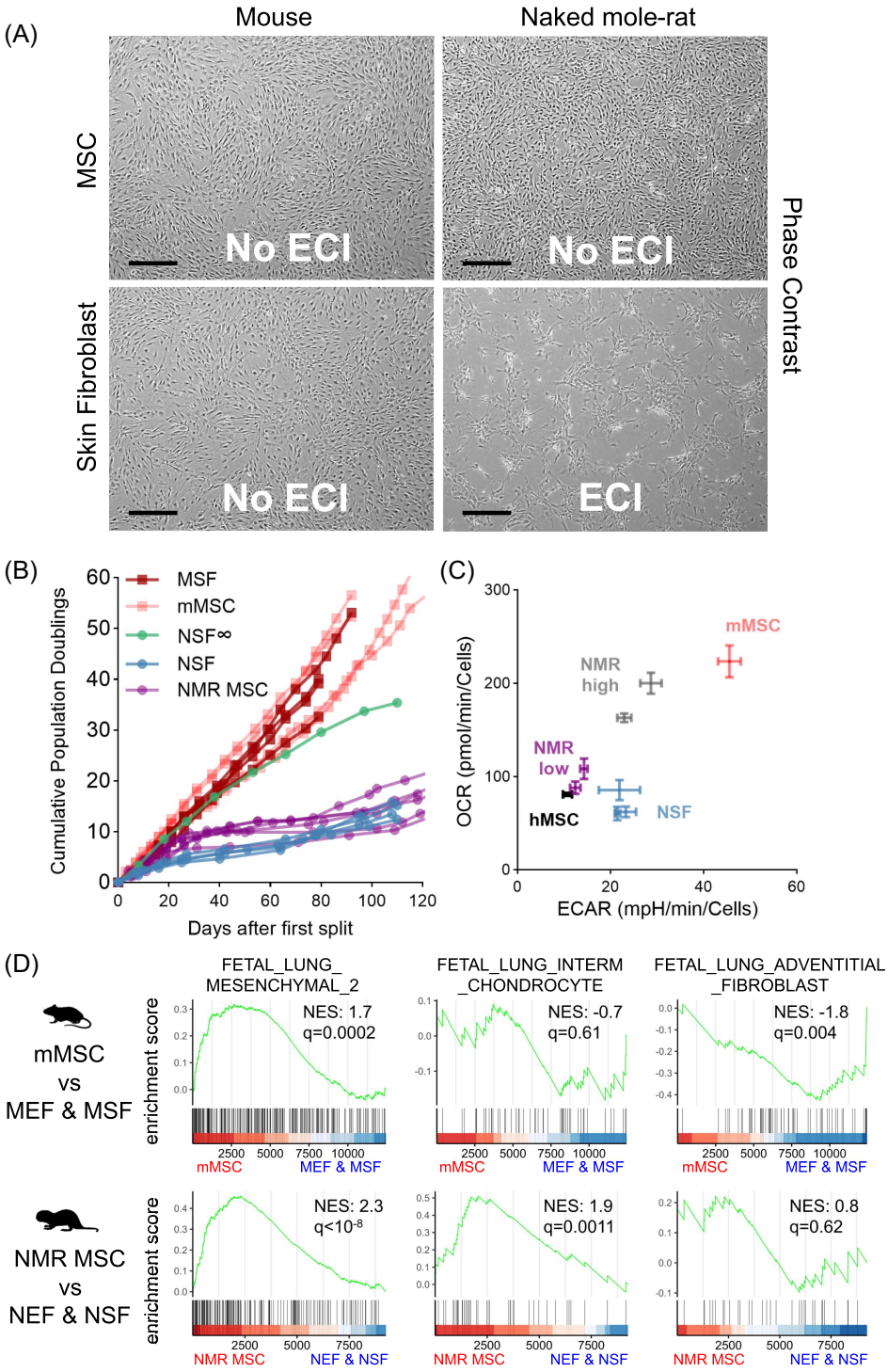

Figure 2. Different in vitro proliferation and metabolic signature between MSCs and skin fibroblasts (SFs). (A) Brightfield microscopy images of MSCs and SFs, 10× magnification objective. ECI, early contact inhibition; scale bars: 200 µm. **(B)** PD curve of MSCs and fibroblasts, one curve per animal. mMSC, mouse MSC; MSF, mouse SF; NSF, NMR SF; NSF ∞, spontaneously immortalized NSF subline. **(C)** Seahorse assay across species and cell types. ECAR, extracellular acidification rate; hMSC, human MSC; mMSC, mouse MSC; NMR high, NMR MSCc high-passage number; NMR low, NMR MSCs low-passage number; NSF, NMR SFs; OCR, oxygen consumption rate. Each cell type, n = 3; error bars represent SD. **(D)** GSEA profiles for cell type-specific signatures from single-cell RNA sequencing (RNA-Seq) annotation gene sets of mMSC versus MSF and MEF (top row) or NMR MSC versus NSF and NEF (bottom row). NES, normalized enrichment score; q, adjusted p value (FDR). MEF, mouse embryonic fibroblast; NEF, NMR embryonic fibroblast. See also **Figures S2–S3**.

weight, while mouse MSCs did not produce detectable HA in vitro.

Next, we applied Seahorse to compare metabolic hallmarks across fibroblasts and MSCs (Fig. 2C). NMR MSCs at low passage before their in vitro growth arrest had very similar OCRs and ECAR to human MSCs, while both rates strongly increased in high-passage NMR MSCs which emerged from the temporary cell cycle arrest. NSFs showed comparable glycolytic activity,

measured through ECAR, as the high-passage NMR MSCs, while their respiratory capacity quantified by OCR was slightly lower than that of human MSCs. Mouse MSCs displayed the highest metabolic activity, corresponding to their proliferative phenotype (Fig. 2C).

To determine cell type-specific differences at the transcriptional level, we compared the gene expression profiles of NMR and mouse MSCs with those of SFs from corresponding species generated in our previous studies[53]. Both NMR and mouse MSCs clustered apart from embryonic and SFs within the first leading dimension (**Fig. S2B,C**), demonstrating distinct gene expression profiles between MSCs and fibroblasts. When we applied a customized gene set collection for GSEA, both mouse and NMR MSCs strongly enriched for the same gene set of a mesenchymal cell fraction from murine fetal lungs (Fig. 2D), while SFs from either species were negatively associated with this gene set (**Fig. S2D**). Interestingly, among 35 leading edge genes of the mesenchymal cell set common between both species, and predominantly comprising genes associated with mitosis and proliferation, *HAPLN1* had the highest expression in NMR MSCs but was strongly downregulated in mouse cells (**Fig. S2E**). *HAPLN1* (hyaluronan and proteoglycan link protein 1) is an ECM component that cross-linking proteoglycan moieties with HA, thereby conferring compression resistance to tissues[54]. This result suggests that *HAPLN1* may contribute to ECM formation in NMR BM through *HAPLN1* production. Furthermore, NMR MSCs also enriched for an interim chondrocyte cell population, which was not significant in mouse MSCs and points toward a transcriptomic trend toward chondrocytic differentiation potential, which was inversely expressed in NSFs (**Fig. S2D**). By contrast, mouse MSC gene expression profiles were significantly depleted for a gene set of adventitial fibroblasts, which was enriched in MSFs (Fig. 2D; **Fig. S2D**). Collectively, our results show that NMR MSCs do not feature contact inhibition in cell culture and have distinct metabolic and transcriptomic features compared to fibroblasts.

CD90/THY1 is marker of NMR MSCs

The core characteristics defining MSCs include plastic adherence under standard culture conditions, the capacity to differentiate into osteoblasts, adipocytes, and chondrocytes in vitro, and the expression of Endoglin (*CD105*), *CD73*, and *THY1* (*CD90*), with a concurrent lack of expression of *CD45*, *CD34*, *CD14* or *CD11b*, *CD79a* or *CD19*, and *HLA-DR*[10]. We previously reported crossspecies reactive antibody staining of CD34 and Thy1.1 protein as surface markers of HSPCs in NMRs[55]. Here, we tested whether *THY1/CD90* is a marker for NMR MSCs. In mice, BM MSCs are isolated by flow cytometry through successive labeling of lineage-negative, $CD146^-/CD166^-$, $CD90.2^+/Sca\text{-}1^+$ cells *in vivo* (**Fig. S3A**). Mouse MSCs grown from bone shards in culture (Fig. 1B) are negative for lineages, *CD146* and *CD166*; however, their immunophenotype for *Sca-1/CD90.2* deviates from *in vivo*, although roughly half of the cells are double positive for the two stem cell markers (Fig. 3A). Since most monoclonal antibodies for the above markers are not available for NMR cells, we used Thy1.1 as a potential positive MSC marker and *CD34* as an exclusion marker. Strikingly, NMR MSCs from neonatal animals showed up to 70% $Thy1.1^+/CD34^-$ low-passage cells, whereas adult NMR MSCs grown from bone material comprised significantly fewer $Thy1.1^+$ cells (Fig. 3B,C). This could be explained by larger stem cell fractions with higher regenerative potential during early development. However, using single-cell plating to determine colony formation frequencies, we did not detect a difference between neonatal and adult NMR MSC isolates (Fig. 3D). Although neonatal MSCs initially grew faster and reached higher PDs than adult MSCs, they also underwent a temporary growth arrest, from which proliferating cells re-emerged (Fig. 3E). Using a fluorescent probe to detect senescent cells by flow cytometry (C12FDG)[56], we found that neonatal MSCs had substantially less galactosidase activity than adult MSCs from NMR BM, whereas mouse MSCs showed the highest senescence-associated fluorescence (**Fig. S3B**). When we separated $Thy1.1^+$ from $Thy1.1^-$ neonatal MSCs through sorting, we saw slightly higher PDs at the same timepoints for $Thy1.1^+$ cells (**Fig. S3C**). We observed a drastic decrease in Thy1.1 levels during the initial growth of $Thy1.1^+$-sorted cells. When Thy1.1+ cells decreased to 20%, Thy1.1 levels stabilized and cells underwent growth arrest, indicating that the cell cycle arrest is associated with the drop in Thy1.1 expression (**Fig. S3D**). In summary, we showed that neonatal and adult NMR MSCs express the *CD90/THY1* surface marker at frequencies corresponding to their ontogenetic stages.

Tri-lineage differentiation potential of mouse and NMR MSCs

The tri-lineage differentiation potential, including osteogenic, adipogenic, and chondrogenic lineages, is a defining hallmark for the therapeutical application of MSCs. Here we used standard in vitro differentiation cocktails derived from multiple reports[17,57] and described in the Methods section to test if NMR MSCs can be differentiated along these lineages (Fig. 4).

To assess osteogenic potential, we used an OIM and measured AP activity and mineralization content by Van Kossa staining. Mouse MSCs at low passage (P4) displayed stronger basal AP activity than MSFs (Fig. 4A). AP staining markedly increased in mouse MSCs but not in mouse fibroblasts in OIM media (Fig. 4A). Conversely, MSFs did not show positive Van Kossa staining, while MSCs were positive and increased mineralization upon treatment with PMN, a small-molecule sonic hedgehog (Shh) pathway activator promoting osteogenic differentiation in MSCs[58]. Similarly, human MSCs at P4 increased AP staining in OIM and boosted mineralization upon treatment with PMN (Fig. 4B). NMR MSCs at low passage showed lower basal AP activity compared to mouse MSCs; however, in OIM media, NMR MSCs displayed the strongest AP staining among all cells tested (Fig. 4C). Strikingly, NSFs were neither positive for AP nor Van Kossa under any conditions. Moreover, NMR MSCs progressively lost osteogenic potential upon prolonged culture, while predominantly growth-arrested and thus <50% confluent P7 cells showed few AP-positive speckles of low staining intensity from colonies, which increased in frequency but not in AP staining intensities from the monolayers of fully confluent cycling P14 cells. Consistently, only low-passage P4 NMR MSCs gave rise to mineralized culture areas under OIM conditions.

To assess chondrogenic potential, we used a CIM to induce the formation of a chondroid from a cell sediment in round-bottom tubes[59] and visualized chondrification efficiency by Alcian Blue Hematoxylin Orange G (ABH-OG) staining for bone and cartilage. Mouse MSCs grown in CIM formed areas of secreted glycosylaminoglycans and proteoglycans stained by ABH-OG, which appeared less nucleated in a corresponding Hematoxylin Eosin (H&E) staining than control sections lacking cartilage secretion

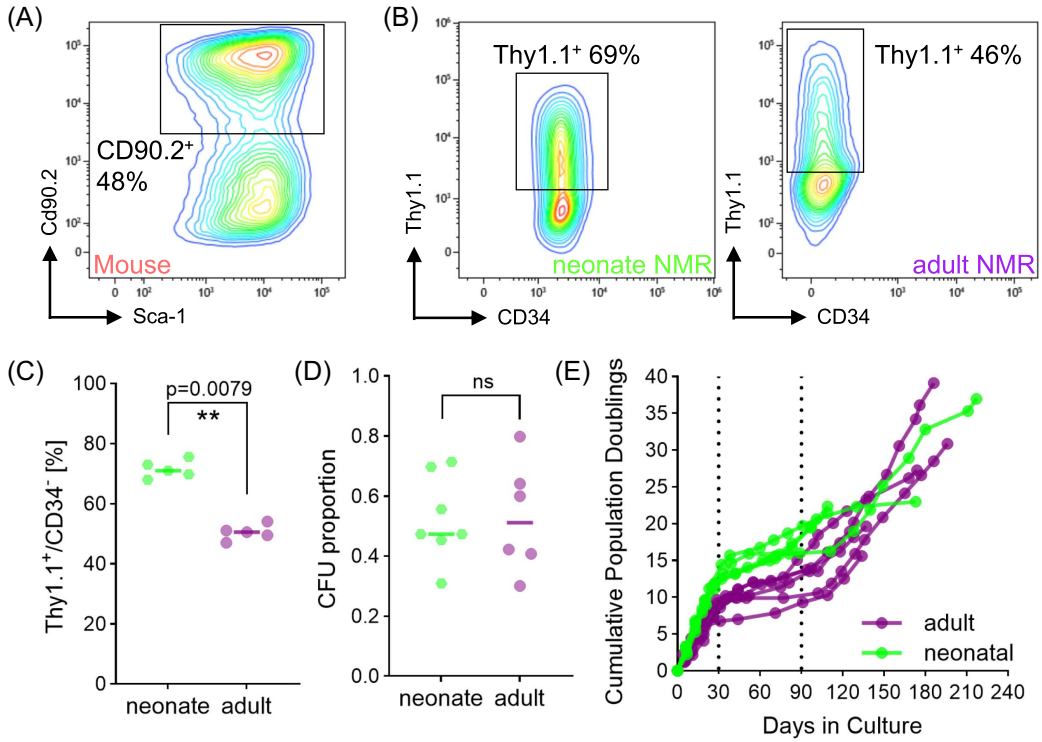

Figure 3. CD90/THY1 in adult and neonatal MSCs. (A) FACS gating of viable LIN$^-$/CD146$^-$/CD166$^-$ cells from mouse MSC cultures. Mouse LIN: *CD11b*, *Gr-1*, *CD3e*, *B220*, and *TER119*. **(B)** FACS gating of viable LIN$^-$ cells from neonate (left) or adult (right) NMR MSC cultures. NMR LIN: *CD11b*, *CD18*, *CD90*, and *CD125*. **(C)** Frequencies of cell populations across ontogenic NMR MSC cultures. P values obtained from the Mann-Whitney rank sum test; n = 5. **(D)** Frequencies of CFU-F across ontogenic NMR MSC cultures. Adult, n = 6; CFU-F, colony-forming unit fibroblast; neonate, n = 7; P values obtained from the Mann-Whitney rank sum test. **(E)** PD curve of primary neonatal or adult NMR MSC cultures; highlighted by two dotted verticals is the average temporary growth arrest period of NMR MSCs. See also **Figure S4**.

(Fig. 4D). The H&E sections of NMR MSCs differentiated in CIM media did show areas with larger nucleated cells surrounded by an ECM instead of densely packed cells in control media; however, the ABH-OG staining failed to detect a clear signal of stained glycan deposits (Fig. 4E). Since the CIM contains recombinant human TGFB3 as a differentiation promoting cytokine, it is possible that NMR MSCs require the NMR homolog or additional factors to complete chondrification in vitro.

To assess adipogenic potential, we cultured MSCs in AIM, followed by visualization of adipocytic differentiation products through Oil Red staining. Mouse MSCs at P4 did not show lipid formation in control or AIM media; however, the addition of Rosiglitazone or Indomethacin to boost adipose differentiation led to the formation of Oil Red positive cells in AIM media (Fig. 4F). None of these conditions produced a positive signal from NMR MSCs. The AIM contains insulin as a critical component, while an insulin insensitivity in response to glucose feeding has been reported in NMRs[60], which may in part explain the inefficient adipogenic in vitro differentiation. In summary, NMR MSCs showed full capacity for osteogenic differentiation. However, under differentiation conditions used for mouse and human MSCs comprising highly similar key reagents[17,57], NMR cells did not secrete cartilage glycans upon chondrogenic differentiation conditions and were refractory to adipogenic differentiation.

NMR MSCs are hypersensitive to Hedgehog signaling

The application of PMN, an agonist of the hedgehog signaling pathway, to increase calcification of osteogenic differentiation cultures was successful for mouse and human MSCs (Fig. 4A,B). However, when we used this compound at the same concentration to boost osteogenic differentiation in NMR MSCs, we repeatedly obtained no signal in either AP or van Kossa stainings (data not shown). We then checked the cultures using regular brightfield microscopy and observed a complete growth arrest as early as day 5 of treatment (Fig. 5A). NMR MSCs showed a sharp decline in cell viability at 1-μM PMN (Fig. 5B). Notably, the luminescent cell viability assay measures substrate conversion through cellular ATP, which is reduced in dead or apoptotic cells; however, non-cycling but otherwise live cells will collectively convert less substrate per well as compared to dividing cells. Indeed, quantification of apoptosis through Annexin V staining did not show marked cell death in NMR MSCs treated with 1-μM PMN (Fig. 5C). Importantly, mouse MSCs showed higher tolerance to PMN, and cycle exit occurred at 10 μM. Fibroblasts of both species tolerated higher doses of PMN (Fig. 5B).

Considering these results, we asked whether hedgehog (Shh) pathway inhibition could potentially increase proliferation. For this, we used cyclopamine, a natural steroidal alkaloid binding to and inhibiting the Shh pathway receptor SMO, thereby inhibiting its downstream cascade. Cyclopamine pharmacokinetics in MSFs and NSFs were almost identical, displaying overt toxicity at 33 μM (Fig. 5D). Annexin V staining confirmed that this effect resulted from apoptosis and cell death in both NMR MSCs and NSFs (Fig. 5E; **Fig. S3E**). In summary, we found a hypersensitivity for both activation and inhibition of the Shh pathway in NMR MSCs, responding to 3–10-fold lower concentrations of the corresponding drugs.

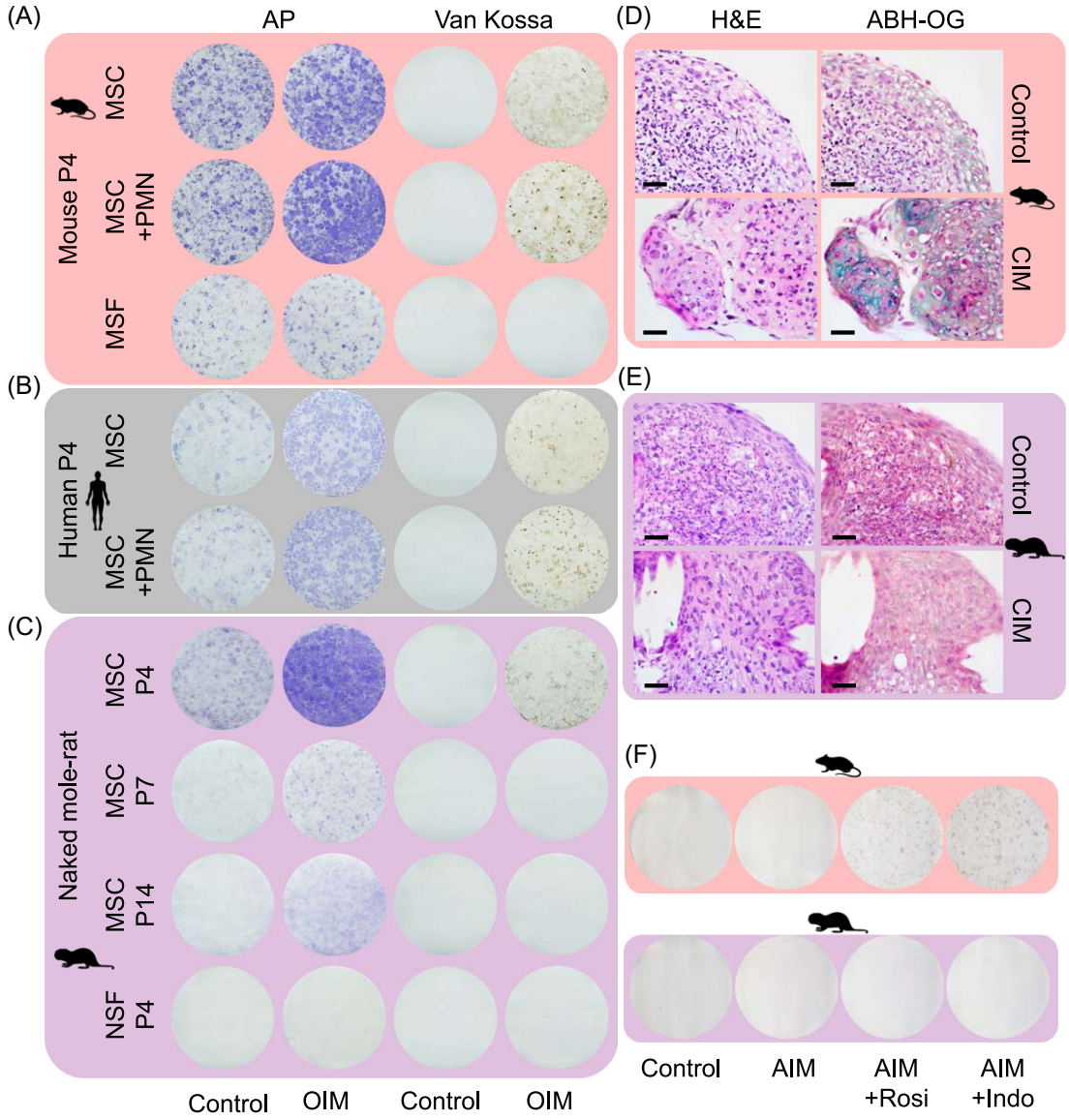

Figure 4. Tri-lineage differentiation capacity of mouse and NMR MSCs. (A) Micrographs of mouse osteogenic differentiation cultures at passage 4. AP, alkaline phosphatase staining measured 2 weeks post-induction; control, basal MSC growth medium; OIM, osteogenic induction cocktail; PMN, purmorphamine; Van Kossa, Van Kossa mineralization staining measured 4 weeks post-induction. Each image is a whole-well scan of stained six-well plates. **(B)** Micrographs of human osteogenic differentiation cultures at passage 4. **(C)** Micrographs of NMR osteogenic differentiation cultures at the indicated passage numbers. **(D)** Microsections of mouse chondroid cultures. ABH-OG, Alcian Blue Hematoxylin/Orange G staining; CIM, chondrogenic induction cocktail; H&E, Hematoxylin Eosin staining. 100× magnification objective; scale bar: 20 μm; arrows indicate extracellular glycan deposits. **(E)** Microsections of NMR chondroid cultures, same magnification as mouse. **(F)** Micrographs of Oil Red O stained mouse (top) and NMR (bottom) adipogenic differentiation cultures. AIM, adipogenic induction cocktail; Indo, Indomethacin; Rosi, Rosiglitazone.

Prolonged cell culture leads to premature senescent phenotypes in NMR MSCs

To characterize the cell cycle arrest displayed by NMR MSCs, we examined MSCs at different stages of proliferation: fresh MSCs that just emerged from bone tissue and formed clusters of proliferating cells; low-passage MSCs (passage 1–5); medium-passage cells (passage 6–8); and high-passage cells (passage 8–10). NMR MSC proliferation rate steadily decreased until passage 4–5, during which few cells stained positive for the senescence marker β-Galactosidase (**Fig. S4A,B**). Medium-passage cells appeared enlarged and stopped dividing, with a higher proportion of β-Galactosidase positive cells (**Fig. S4C**). High-passage cells displayed clonal outgrowth of pleomorphic cells throughout passages 10–20 (**Fig. S4A,D**).

Next, we compared the bulk transcriptomes of the various passage stages described above. The supervised passage group clusters distinctly mapped to nonoverlapping areas in a t-distributed Stochastic Neighbor Embedding (t-SNE) projection (Fig. 6A) and consequently featured overexpressed gene sets specific for each proliferation stage (**Fig. S5A**). Functional annotation using GSEA for fresh MSCs yielded strong enrichment of proliferation-associated pathways such as G2M checkpoint and *E2F/MYC* targets (Fig. 6B), exemplified through specific overexpression of mitotic effectors and regulator genes such as lambda DNA polymerase (*POLL*), *PIMREG*, *PCLAF*, and *RBP1* (**Fig. S5A**). Moreover, positive enrichment scores for glycolysis and MTORC1 signaling, as well as cytoprotective pathways for DNA repair and unfolded protein response (UPR), were obtained for fresh NMR MSCs (Fig. 6B).

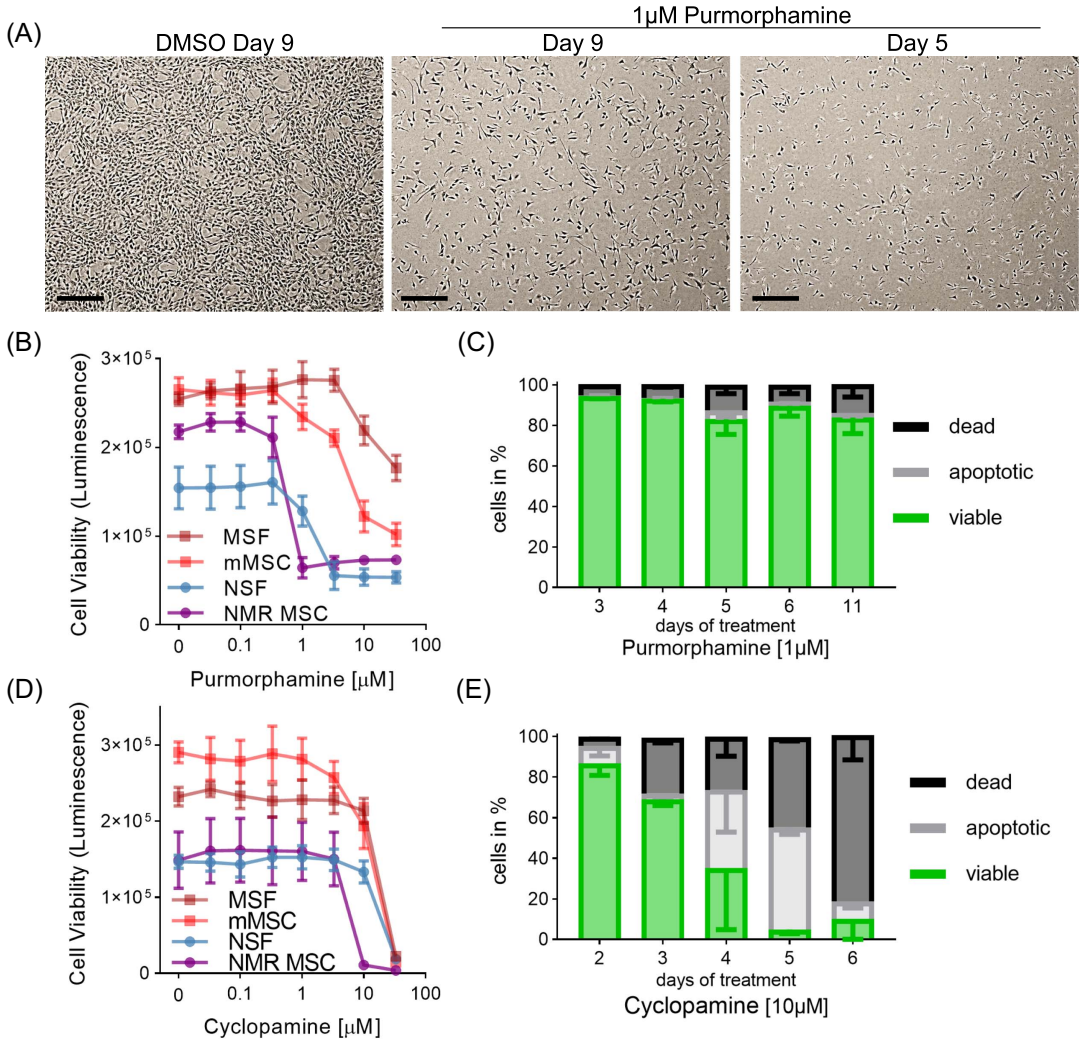

Figure 5. Sensitivity to hedgehog signaling perturbation in NMR MSCs. (A) Brightfield microscopy images of NMR MSCs treated with purmorphamine (PMN); 10× magnification objective; scale bars: 200 μm. **(B)** Cell viability at day 6 of culture or treatment with increasing PMN doses; error bars represent SD. mMSC, mouse MSC; MSF, mouse SF; NSF, NMR SF. **(C)** AnnexinV/DAPI staining of NMR MSCs at different endpoints post 1-μM PMN treatment. **(D)** Cell viability at day 6 of culture or treatment with increasing cyclopamine doses; error bars represent SD. **(E)** AnnexinV/DAPI staining of NMR MSCs at different endpoints post 10-μM cyclopamine treatment. See also **Figure S4**.

We validated the functional annotation using the gene ontology (GO) biological process gene set collection, which enriched for multiple biosynthetic processes along with further DNA repair-associated terms (**Fig. S5B**), supporting the notion that fresh MSC isolates represent intact regenerative and metabolic molecular processes and showed a transcriptional response to serum stimulation in vitro. Low-passage cell transcriptomes displayed downregulated energy-related pathways (Fig. 6B), namely OXPHOS and membrane_lipid_metabolic_process, along with enrichment for myogenic differentiation signatures through overexpression of *MYOG*, *MYOD1*, and *PAX7* (**Figs. S5A and S6A**). Strikingly, growth arrested intermediate passage cells scored high for multiple high-level inflammatory pathways, including *STAT* and *TNFα* signaling, interferon response, and complement cascade (Fig. 6B). Consistently, we found enriched GO categories for Toll receptor signaling, innate immune response, and interleukin production pathways, together with p53 signaling and oxidative stress response signatures (**Fig. S6B**), highlighted through overexpression of *IL6*, *CSF2*, *NOS2*, and *NLRP3* in intermediate passage cells. Moreover, by feature extraction from the SenMayo gene set predicting senescence-associated patterns and senescent cells[61], we found a global trend of increasing expression in most signature genes with increasing time under culture (Fig. 6C; **Fig. S7**). By contrast, high-passage cells displayed exclusively negative associations with mitotic pathways and MTOR signaling despite overriding temporary cell cycle arrest (Fig. 6B). Indeed, cellular biosynthesis processes, DNA damage response, and UPR terms were downregulated in high-passage cells (**Fig. S6C**). Consistently, subsetting the cell cycle gene collection from the murine cyclone classifier list into common and stage-specific gene blocks yielded a clear overexpression of the majority of genes from any block in fresh MSCs (**Fig. S8A**)[62]. Since high-passage cells continuously proliferated in vitro, albeit with a lower PD rate than fresh cells (Fig. 3E), we checked the expression of selected cyclins and checkpoint kinases across passaging stages. Cyclin A1 (*CCNA1*) and *E2F1* expression sharply declined during the transition from fresh to low-passage cells before rising again through intermediate passage to high-passage cells (Fig. 6D). Similar trends were obtained for *CDK2* and *CDC25B* (**Fig. S8B**). However, *CDK1* mRNA constantly decreased, whereas cyclin D1 (*CCND1*) expression steadily increased, and

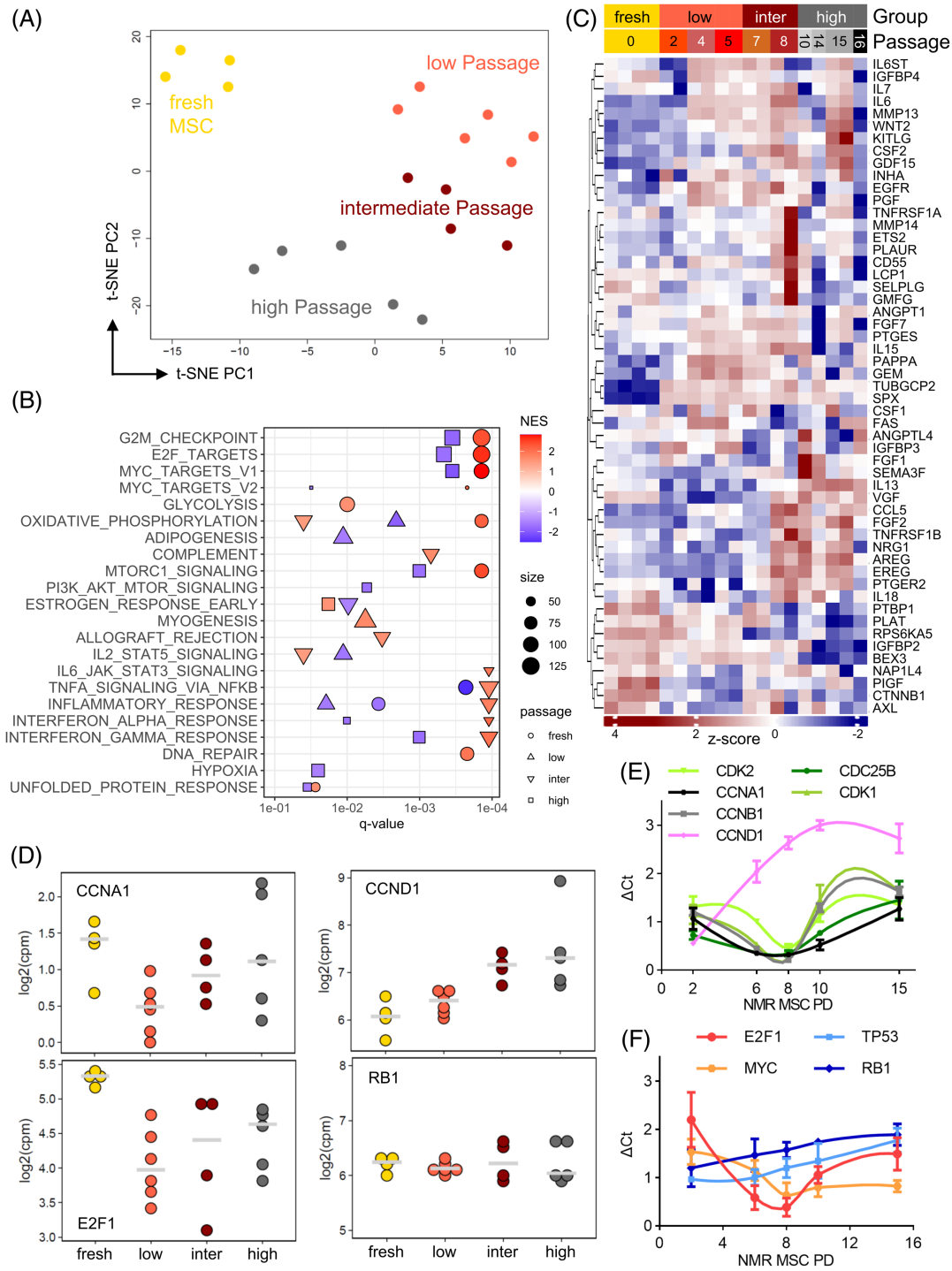

Figure 6. Premature senescence in cultured NMR MSCs. (A) t-SNE mapping of NMR MSC bulk transcriptomes clustered according to time in culture. Fresh NMR MSCs, no passage; low-passage MSCs, low passage; middle/medium-passage MSCs, intermdiate passage; high-passage MSCs, high passage. **(B)** GSEA between four clusters of passage time using the MSigDb hallmark gene set collection. NES, normalized enrichment core; q value, adjusted p value (FDR); size, the number of gene overlaps between query signature and gene set. **(C)** NMR ortholog expression of the SenMayo sensescence gene set across passage time from voom-transformed, z-score-centered reads. **(D)** Expression of *CCNA1*, *CCND1*, *E2F1*, and *RB1* genes from bulk RNA-Seq transcriptomes; Log2(CPM), log-transformed counts per million. Quantitative PCR validation of **(E)** selected cell cycle regulators and **(F)** tumor suppressor or oncogenes at different timepoints in culture. ΔCt, gene of interest Ct, normalized to housekeeping genes B2M and ACT Ct. See also **Figures S4–S7**.

tumor suppressor *RB1* levels were largely maintained over time in culture. Subsequent qPCR validation fortified only *CCND1* expression as constantly increasing with time, while all other cell cycle regulators would dip expression levels around the temporary growth arrest, while tumor suppressor genes p53 and Rb were slightly elevated toward high-passage numbers (Fig. 6E,F).

Conclusively, we showed that NMR MSCs underwent premature senescence at PD 6–8. The growth arrested cells had many

features of senescence. However, the arrest was temporary, and "immortalized" clones emerged, showing elevated oxidative stress, replicative stress, and tumor suppressive signaling.

Discussion

We performed the first isolation and characterization of bone-marrow-derived MSCs from the long-lived NMR. NMR MSCs displayed the *CD90/THY1* surface marker, which is a consensus marker for the MSC state[10], with higher expression in neonatal MSCs. Thy1.1 expression progressively diminished with time in culture, in line with the premature senescence phenotype acquired with prolonged in vitro cultivation. We further showed the myeloid and fibroblastic marker *CD68* was specifically down-regulated in NMR MSCs, while *CD34* was negative on both NMR and human MSCs, supporting the identity of NMR BM-derived stromal cells as MSCs.

Tri-lineage differentiation capacity is a major hallmark of the MSC cell state and a consensus criterion for therapeutic MSC applications[10]. Our results suggest that NMR MSCs have a bias toward osteogenic cell fate and limited differentiation potential for adipogenic fate. Notably, we found the leptin receptor (*LEPR*) to be overexpressed in human MSCs, which we collected from adult donors, and not expressed in NMR MSCs (**Fig. S1F**). Leptin is produced by adipocytes, whereas *LEPR* has been shown to identify BM-MSCs in mice[63], is responsible for fate decision between adipogenic and osteogenic lineages, and promotes BM innervation through *NGF* secretion[64,65]. In human cells, leptin treatment increased the survival of transplanted MSCs into myocardial infarction sites[66]; however, primary LEPR^{hi} human MSCs show a decreased number of generations in culture and advanced biological age[67]. The lack of defined conditions to induce adipogenic differentiation in NMR cells warrants caution in drawing conclusions regarding fate decision biases.

Interestingly, in vitro MSCs from NMR and two other mole-rat species (BMR and DMR) entered a stage of prolonged growth arrest similar to human MSCs and sharply distinct from the rapid proliferation displayed by MSCs from mouse, rat, and bat. This growth arrest may indicate hypersensitivity to culture conditions and overstimulation by fetal calf serum, leading to activation of tumor-suppressor signaling. Consistently, all three mole-rat species are characterized by very low cancer incidence compared to mouse and rat[68–73]. Human MSC cultures eventually become senescent with time, whereas mouse MSCs display accelerated proliferation. The cell growth phenotype of cultured NMR MSCs appears to incorporate both phenotypes of human and mouse MSCs in a staged fashion, such as an initial growth period followed by a temporary growth arrest resembling features of senescence, followed by clonal re-entering of the cell cycle. Human cells have evolved several checkpoint mechanisms, which are lacking in murine cells[74]. For example, human terminally differentiated cells do not express telomerase; instead, they evolved replicative senescence as a tumor suppressor mechanism to compensate for higher cancer incidence in large-bodied animals[75]. The human MSC in vitro growth phenotype is likely a combination of the induction of replicative senescence and premature senescence due to cell culture stress. While long-lived small-bodied animals like NMRs do not repress telomerase or undergo replicative senescence, they evolved an array of alternative tumor suppressor mechanisms manifesting in slow cell growth in vitro[51]. NMR MSCs enter a senescence-like state due to the stress of cell culture but not telomere shortening. We hypothesize that after a while, these non-telomeric mechanisms are overridden due to constant growth factor signaling from serum in the culture media which may be associated with genetic or epigenetic changes at the single-cell level.

Unexpectedly, NMR MSCs did not display the ECI characteristic of NMR fibroblasts and expressed HA of lower molecular weight. This is consistent with the faster proliferation of the NMR MSCs and their propensity to give rise to immortalized clones after a period of stasis. While these features may lead to a higher chance of malignant transformation, they may at the same time enhance the regenerative properties of the NMR MSCs.

The hypersensitivity of NMR MSCs to Shh pathway modulation suggests an intricate balance essential to maintain MSC identity. Indeed, it has been shown that PMN-induced expression of pro-angiogenic factors such as activin A, angiogenin, and angiopoietin 1 in Wharton's jelly-derived MSCs[76], whereas *SHH* overexpression in osteoarthritic MSCs led to SASP and chondrocyte apoptosis[77].

The distinct gene expression profiles of NMR MSCs suggest a unique regulatory landscape. No *CXCL12* production by NMR MSCs points toward one or multiple separate cell types in the marrow to support HSPC homing, which is conserved in NMRs[37,78]. The diminished levels of DNA methylases may be relevant for the cancer resistance of these species. We recently showed that in the distantly related BMR (*Spalax spp*), DNMT1 levels are very low, and the resulting loss of retrotransposon silencing during hyperplasia with subsequent cGAS-STING pathway induction is co-opted as a tumor suppressor mechanism[53]. The elevated expression of *SIRT1/2/3/6* in NMR MSCs raises intriguing questions about the role of these genes in conferring NMR's exceptional longevity. In mice, *SIRT1*-defective MSCs have lower osteogenic capacity, which could be rescued by mutating known acetylation sites in β-catenin[79]. Moreover, in humans and rats, *SIRT1* activity ameliorated MSC senescence upon prolonged culture in vitro[80,81]. SIRT2 is the most abundant sirtuin in adipocytes, and its overexpression prohibits adipogenesis[82], which is in line with the lack of in vitro adipogenic differentiation in *SIRT2* overexpressing NMR MSCs. *SIRT6* has been shown to co-activate *NRF2*, conferring resistance to oxidative stress in human MSCs[83]. These findings prompt further exploration of the interconnected roles of Sirtuins in MSC maintenance and longevity.

In conclusion, our characterization of NMR MSCs contributes essential insights into the isolation and propagation of a therapeutically relevant stem cell population in this long-lived rodent. The unique attributes of NMR MSCs, including growth arrest, lineage fate biases, and responses to culture conditions, hold potential implications for understanding longevity and cancer resistance.

Acknowledgments

Many thanks to Nancy Corson for naked mole-rat (NMR) colony management and Yulia Ablaeva for general lab support. The authors thank John Ashton for Genomic Research Core support, the Center for Integrated Research Computing (CIRC) at the University of Rochester for providing computational resources and technical support, and the URMC Flow Core for assistance with sorting and Seahorse. This work was supported by grants from the U.S. National Institute on Aging to V.G. and A.S., the Michael Antonov Foundation, the Impetus Grant, and the Milky Way Research Foundation to V.G.

Conflict of Interest

The authors declare no conflict of interest.

Supplementary Materials

Supplemental information can be found online at https://doi.org/10.59368/agingbio.20240029.

References

1. Gorbunova V., Seluanov A., Zhang Z., Gladyshev V.N., & Vijg J. (2014). Comparative genetics of longevity and cancer: Insights from long-lived rodents. *Nat. Rev. Genet.* 531–540. PMID: 24981598; doi: 10.1038/nrg3728.
2. Ruby J.G., Smith M., & Buffenstein R. (2018). Naked mole-rat mortality rates defy Gompertzian laws by not increasing with age. *Elife* **7**, e31157. PMID: 29364116; doi: 10.7554/eLife.31157.
3. Buffenstein R., & Ruby J.G. (2021). Opportunities for new insight into aging from the naked mole-rat and other non-traditional models. *Nat. Aging* 3–4. PMID: 37117998; doi: 10.1038/s43587-020-00012-4.
4. Pride H., Yu Z., Sunchu B., Mochnick J., Coles A., Zhang Y., … Pérez V.I. (2015). Long-lived species have improved proteostasis compared to phylogenetically-related shorter-lived species. *Biochem. Biophys. Res. Commun.* **457**, 669–675. PMID: 25615820; doi: 10.1016/j.bbrc.2015.01.046.
5. Lewis K.N., Wason E., Edrey Y.H., Kristan D.M., Nevo E., & Buffenstein R. (2015). Regulation of Nrf2 signaling and longevity in naturally long-lived rodents. *Proc. Natl. Acad. Sci. U. S. A.* **112**(12), 3722–3727. PMID: 25775529; doi: 10.1073/pnas.1417566112.
6. Azpurua J., Ke Z., Chen I.X., Zhang Q., Ermolenko D.N., Zhang Z.D., … Seluanov A. (2013). Naked mole-rat has increased translational fidelity compared with the mouse, as well as a unique 28S ribosomal RNA cleavage. *Proc. Natl. Acad. Sci. U. S. A.* **110**(43), 17350–17355. PMID: 24082110; doi: 10.1073/pnas.1313473110.
7. Tian X., Azpurua J., Ke Z., Augereau A., Zhang Z.D., Vijg J., … Seluanov A. (2015). INK4 locus of the tumor-resistant rodent, the naked mole rat, expresses a functional p15/p16 hybrid isoform. *Proc. Natl. Acad. Sci. U. S. A.* **112**(4), 1053–1058. PMID: 25550505; doi: 10.1073/pnas.1418203112.
8. Tian X., Azpurua J., Hine C., Vaidya A., Myakishev-Rempel M., Ablaeva J., … Seluanov A. (2013). High-molecular-mass hyaluronan mediates the cancer resistance of the naked mole rat. *Nature* **499**(7458), 346–349. PMID: 23783513; doi: 10.1038/nature12234.
9. Pittenger M.F., Mackay A.M., Beck S.C., Jaiswal R.K., Douglas R., Mosca J.D., … Marshak D.R. (1999). Multilineage potential of adult human mesenchymal stem cells. *Science* **284**(5411), 143–147. PMID: 10102814; doi: 10.1126/science.284.5411.143.
10. Dominici M., Le Blanc K., Mueller I., Slaper-Cortenbach I., Marini F.C., Krause D.S., … Horwitz E.M. (2006). Minimal criteria for defining multipotent mesenchymal stromal cells. The International Society for Cellular Therapy position statement. *Cytotherapy* **8**(4), 315–317. PMID: 16923606; doi: 10.1080/14653240600855905.
11. Najar M., Raicevic G., Fayyad-Kazan H., Bron D., Toungouz M., & Lagneaux L. (2016). Mesenchymal stromal cells and immunomodulation: A gathering of regulatory immune cells. *Cytotherapy* **18**(2), 160–171. PMID: 26794710; doi: 10.1016/j.jcyt.2015.10.011.
12. English K., & Mahon B.P. (2011). Allogeneic mesenchymal stem cells: Agents of immune modulation. *J. Cell. Biochem.* **112**(8), 1963–1968. PMID: 21445861; doi: 10.1002/jcb.23119.
13. Le Blanc K., & Mougiakakos D. (2012). Multipotent mesenchymal stromal cells and the innate immune system. *Nat. Rev. Immunol.* **12**(5), 383–396. PMID: 22531326; doi: 10.1038/nri3209.
14. Stolzing A., Jones E., McGonagle D., & Scutt A. (2008). Age-related changes in human bone marrow-derived mesenchymal stem cells: Consequences for cell therapies. *Mech. Ageing Dev.* **129**(3), 163–173. PMID: 18241911; doi: 10.1016/j.mad.2007.12.002.
15. Coppé J.P., Patil C.K., Rodier F., Sun Y., Muñoz D.P., Goldstein J., … Campisi J. (2008). Senescence-associated secretory phenotypes reveal cell-nonautonomous functions of oncogenic RAS and the p53 tumor suppressor. *PLoS Biol.* **6**(12), e301. PMID: 19053174; doi: 10.1371/journal.pbio.0060301.
16. Ke Z., Vaidya A., Ascher J., Seluanov A., & Gorbunova V. (2014). Novel husbandry techniques support survival of naked mole rat (heterocephalus glaber) pups. *J. Am. Assoc. Lab. Anim. Sci.* **53**(1), 89–91. PMID: 24411785.
17. Zhu H., Guo Z.K., Jiang X.X., Li H., Wang X.Y., Yao H.Y., … Mao N. (2010). A protocol for isolation and culture of mesenchymal stem cells from mouse compact bone. *Nat. Protoc.* **5**(3), 550–560. PMID: 20203670; doi: 10.1038/nprot.2009.238.
18. Seluanov A., Vaidya A., & Gorbunova V. (2010). Establishing primary adult fibroblast cultures from rodents. *J. Vis. Exp.* **44**, e2033. PMID: 20972406; doi: 10.3791/2033.
19. Cristofalo V.J., Volker C., Francis M.K., & Tresini M. (1998). Age-dependent modifications of gene expression in human fibroblasts. *Crit. Rev. Eukaryot. Gene Expr.* **8**(1), 43–80. PMID: 9673450; doi: 10.1615/critreveukargeneexpr.v8.i1.30.
20. Cahu J., & Sola B. (2013). A sensitive method to quantify senescent cancer cells. *JoVE* e50494. Retrieved from https://www.jove.com/t/50494.
21. Zhao Y., Tyshkovskiy A., Muñoz-Espín D., Tian X., Serrano M., De Magalhaes J.P., … Gorbunova V. (2018). Naked mole rats can undergo developmental, oncogene-induced and DNA damage-induced cellular senescence. *Proc. Natl. Acad. Sci. U. S. A.* **115**(8), 1801–1806. PMID: 29432174; doi: 10.1073/pnas.1721160115.
22. Bolger A.M., Lohse M., & Usadel B. (2014). Trimmomatic: A flexible trimmer for Illumina sequence data. *Bioinformatics* **30**, 2114–2120. PMID: 24695404; doi: 10.1093/bioinformatics/btu170.
23. Patro R., Duggal G., Love M.I., Irizarry R.A., & Kingsford C. (2017). Salmon provides fast and bias-aware quantification of transcript expression. *Nat. Methods* **14**(4), 417–419. PMID: 28263959; doi: 10.1038/nmeth.4197.
24. Lu J.Y., Simon M., Zhao Y., Ablaeva J., Corson N., Choi Y., … Gorbunova V. (2022). Comparative transcriptomics reveals circadian and pluripotency networks as two pillars of longevity regulation. *Cell Metab.* **34**(6), 836–856.e5. PMID: 35580607; doi: 10.1016/j.cmet.2022.04.011.
25. Korotkevich G., Sukhov V., Budin N., Shpak B., Artyomov M.N., & Sergushichev A. (2021). Fast gene set enrichment analysis. *bioRxiv* 060012. Retrieved from http://biorxiv.org/content/early/2021/02/01/060012.abstract.
26. Plaisier S.B., Taschereau R., Wong J.A., & Graeber T.G. (2010). Rank–rank hypergeometric overlap: Identification of statistically significant overlap between gene-expression signatures. *Nucleic Acids Res.* **38**(17), e169–e169. PMID: 20660011; doi: 10.1093/nar/gkq636.
27. Schellenberg A., Lin Q., Schüler H., Koch C.M., Joussen S., Denecke B., … Wagner W. (2011). Replicative senescence of mesenchymal stem cells causes DNA-methylation changes which correlate with repressive histone marks. *Aging* **3**, 873–888. PMID: 22025769; doi: 10.18632/aging.100391.
28. Li Y., Wu Q., Wang Y., Li L., Bu H., & Bao J. (2017). Senescence of mesenchymal stem cells (review). *Int. J. Mol. Med.* **39**(4), 775–782. PMID: 28290609; doi: 10.3892/ijmm.2017.2912.
29. Yu J., Shi J., Zhang Y., Zhang Y., Huang Y., Chen Z., & Yang J. (2018). The replicative senescent mesenchymal stem / stromal cells defect in DNA damage response and anti-oxidative capacity. *Int. J. Med. Sci.* **15**(8), 771–781. PMID: 30008586; doi: 10.7150/ijms.24635.
30. Simon M., Yang J., Gigas J., Earley E.J., Hillpot E., Zhang L., … Gorbunova V. (2022). A rare human centenarian variant of SIRT6 enhances genome stability and interaction with Lamin A. *EMBO J.* **41**(21), e110393. PMID: 36215696; doi: 10.15252/embj.2021110393.
31. Mao Z., Hine C., Tian X., Van Meter M., Au M., Vaidya A., … Gorbunova V. (2011). SIRT6 promotes DNA repair under stress by activating PARP1. *Science* **332**(6036), 1443–1446. PMID: 21680843; doi: 10.1126/science.1202723.

32. Takasugi M., Ohtani N., Takemura K., Emmrich S., Zakusilo F.T., Yoshida Y., … Gorbunova V. (2023). CD44 correlates with longevity and enhances basal ATF6 activity and ER stress resistance. *Cell Rep.* **42**(9), 113130. PMID: 37708026; doi: 10.1016/j.celrep.2023.113130.

33. Zhao Y., Zheng Z., Zhang Z., Xu Y., Hillpot E., Lin Y.S., … Gorbunova V. (2023). Evolution of high-molecular-mass hyaluronic acid is associated with subterranean lifestyle. *Nat. Commun.* **14**(1), 8054. PMID: 38052795; doi: 10.1038/s41467-023-43623-2.

34. Etienne-Manneville S. (2004). Cdc42 - The centre of polarity. *J. Cell. Sci.* **117**(8), 1291–1300. PMID: 15020669; doi: 10.1242/jcs.01115.

35. Baum C.M., Weissman I.L., Tsukamoto A.S., Buckle A.-M., & Peault B. (1992). Isolation of a candidate human hematopoietic stem-cell population. *Proc. Natl. Acad. Sci. U. S. A.* **89**(7), 2804–2808. PMID: 1372992; doi: 10.1073/pnas.89.7.2804.

36. Hass R., Kasper C., Böhm S., & Jacobs R. (2011). Different populations and sources of human mesenchymal stem cells (MSC): A comparison of adult and neonatal tissue-derived MSC. *Cell Commun. Signal.* **9**, 12 PMID: 21569606; doi: 10.1186/1478-811X-9-12.

37. Emmrich S., Trapp A., Tolibzoda Zakusilo F., Straight M.E., Ying A.K., Tyshkovskiy A., … Gorbunova V. (2022). Characterization of naked mole-rat hematopoiesis reveals unique stem and progenitor cell patterns and neotenic traits. *EMBO J.* **41**(15), e109694. PMID: 35694726; doi: 10.15252/embj.2021109694.

38. Zannettino A.C., Bühring H.-J., Niutta S., Watt S.M., Ann Benton M., & Simmons P.J. (1998). The sialomucin CD164 (MGC-24v) is an adhesive glycoprotein expressed by human hematopoietic progenitors and bone marrow stromal cells that serves as a potent negative regulator of hematopoiesis. *Blood* **92**(8), 2613–2628. PMID: 9763543; doi: 10.1182/blood.V92.8.2613.

39. Pellin D., Loperfido M., Baricordi C., Wolock S.L., Montepeloso A., Weinberg O.K., … Biasco L. (2019). A comprehensive single cell transcriptional landscape of human hematopoietic progenitors. *Nat. Commun.* **10**, 2395. PMID: 31160568; doi: 10.1038/s41467-019-10291-0.

40. Kunz-Schughart L.A., Weber A., Rehli M., Gottfried E., Brockhoff G., Krause S.W., … Kreutz M. (2003). [The "classical" macrophage marker CD68 is strongly expressed in primary human fibroblasts]. *Verh. Dtsch. Ges. Pathol.* **87**, 215–223. PMID: 16888915.

41. La Rocca G., Anzalone R., & Farina F. (2009). The expression of CD68 in human umbilical cord mesenchymal stem cells: New evidences of presence in non-myeloid cell types. *Scand. J. Immunol.* **70**(2), 161–162. PMID: 19630923; doi: 10.1111/j.1365-3083.2009.02283.x.

42. Moll N.M., & Ransohoff R.M. (2010). CXCL12 and CXCR4 in bone marrow physiology. *Expert Rev. Hematol.* **3**(3), 315–322. PMID: 21082982; doi: 10.1586/ehm.10.16.

43. Rajagopal S., Kim J., Ahn S., Craig S., Lam C.M., Gerard N.P., … Lefkowitz R.J. (2010). β-Arrestin- but not G protein-mediated signaling by the "decoy" receptor CXCR7. *Proc. Natl. Acad. Sci. U. S. A.* **107**(2), 628–632. PMID: 20018651; doi: 10.1073/pnas.0912852107.

44. Hartmann T.N., Grabovsky V., Pasvolsky R., Shulman Z., Buss E.C., Spiegel A., … Alon R. (2008). A crosstalk between intracellular CXCR7 and CXCR4 involved in rapid CXCL12-triggered integrin activation but not in chemokine-triggered motility of human T lymphocytes and CD34 + cells. *J. Leukoc. Biol.* **84**(4), 1130–1140. PMID: 18653785; doi: 10.1189/jlb.0208088.

45. Burns J.M., Summers B.C., Wang Y., Melikian A., Berahovich R., Miao Z., … Schall T.J. (2006). A novel chemokine receptor for SDF-1 and I-TAC involved in cell survival, cell adhesion, and tumor development. *J. Exp. Med.* **203**(9), 2201–2213. PMID: 16940167; doi: 10.1084/jem.20052144.

46. Imai T., Hieshima K., Haskell C., Baba M., Nagira M., Nishimura M., … Yoshie O. (1997). Identification and molecular characterization of fractalkine receptor CX3CR1, which mediates both leukocyte migration and adhesion. *Cell* **91**(4), 521–530. PMID: 9390561; doi: 10.1016/S0092-8674(00)80438-9.

47. Lee C.H., Shah B., Moioli E.K., & Mao J.J. (2010). CTGF directs fibroblast differentiation from human mesenchymal stem/stromal cells and defines connective tissue healing in a rodent injury model. *J. Clin. Invest.* **120**(9), 3340–3349. PMID: 20679726; doi: 10.1172/JCI43230.

48. Haniffa M.A., Collin M.P., Buckley C.D., & Dazzi F. (2009). Mesenchymal stem cells: the fibroblasts' new clothes? *Haematologica* **94**(2), 258–263. PMID: 19109217; doi: 10.3324/haematol.13699.

49. Hematti P. (2012). Mesenchymal stromal cells and fibroblasts: A case of mistaken identity? *Cytotherapy* **14**(5), 516–521. PMID: 22458957; doi: 10.3109/14653249.2012.677822.

50. Seluanov A., Hine C., Azpurua J., Feigenson M., Bozzella M., Mao Z., … Gorbunova V. (2009). Hypersensitivity to contact inhibition provides a clue to cancer resistance of naked mole-rat. *Proceedings of the National Academy of Sciences.* **106**(46), 19352–19357. doi: 10.1073/pnas.0905252106.

51. Seluanov A., Hine C., Bozzella M., Hall A., Sasahara T.H.C., Ribeiro A.A.C.M., … Gorbunova V. (2008). Distinct tumor suppressor mechanisms evolve in rodent species that differ in size and lifespan. *Aging Cell* **7**(6), 813–823. PMID: 18778411; doi: 10.1111/j.1474-9726.2008.00431.x.

52. Takasugi M., Firsanov D., Tombline G., Ning H., Ablaeva J., Seluanov A., & Gorbunova V. (2020). Naked mole-rat very-high-molecular-mass hyaluronan exhibits superior cytoprotective properties. *Nat. Commun.* **11**, 2376. PMID: 32398747; doi: 10.1038/s41467-020-16050-w.

53. Zhao Y., Oreskovic E., Zhang Q., Lu Q., Gilman A., Lin Y.S., … Gorbunova V. (2021). Transposon-triggered innate immune response confers cancer resistance to the blind mole rat. *Nat. Immunol.* **22**(10), 1219–1230. PMID: 34556881; doi: 10.1038/s41590-021-01027-8.

54. Spicer A.P., Joo A., & Bowling R.A. (2003). A hyaluronan binding link protein gene family whose members are physically linked adjacent to chrondroitin sulfate proteoglycan core protein genes: The missing links. *J. Biol. Chem.* **278**(23), 21083–21091. PMID: 12663660; doi: 10.1074/jbc.M213100200.

55. Emmrich S., Trapp A., Tolibzoda Zakusilo F., Straight M.E., Ying A.K., Tyshkovskiy A., … Gorbunova V. (2022). Characterization of naked mole-rat hematopoiesis reveals unique stem and progenitor cell patterns and neotenic traits. *EMBO J.* **41**(15), e109694. PMID: 35694726; doi: 10.15252/embj.2021109694.

56. Debacq-Chainiaux F., Erusalimsky J.D., Campisi J., & Toussaint O. (2009). Protocols to detect senescence-associated beta-galactosidase (SA-βgal) activity, a biomarker of senescent cells in culture and in vivo. *Nat. Protoc.* **4**(12), 1798–1806. PMID: 20010931; doi: 10.1038/nprot.2009.191.

57. Ciuffreda M.C., Malpasso G., Musarò P., Turco V., & Gnecchi M. (2016). Protocols for in vitro differentiation of human mesenchymal stem cells into osteogenic, chondrogenic and adipogenic lineages. *Methods Mol. Bio.* 149–158. PMID: 27236670; doi: 10.1007/978-1-4939-3584-0_8.

58. Wöltje M., Böbel M., Heiland M., Beck-Broichsitter B., Al-Dam A., Gröbe A., … Smeets R. (2015). Purmorphamine and oxysterols accelerate and promote osteogenic differentiation of mesenchymal stem cells in vitro. *In Vivo (Brooklyn)* **29**, 247. Retrieved from http://iv.iiarjournals.org/content/29/2/247.abstract.

59. Chen X., McClurg A., Zhou G.-Q., McCaigue M., Armstrong M.A., & Li G. (2007). Chondrogenic differentiation alters the immunosuppressive property of bone marrow-derived mesenchymal stem cells, and the effect is partially due to the upregulated expression of B7 molecules. *Stem Cells* **25**, 364–370. PMID: 17068184; doi: 10.1634/stemcells.2006-0268.

60. Buffenstein R., Kang J., & Biney A. (2007). Glucose tolerance and insulin sensitivity in an extremely long-living rodent, the naked mole-rat. *FASEB J.* **21**(6), A1423–A1423. doi: 10.1096/fasebj.21.6.A1423-c.

61. Saul D., Kosinsky R.L., Atkinson E.J., Doolittle M.L., Zhang X., LeBrasseur N.K., … Khosla S. (2022). A new gene set identifies senescent cells and predicts senescence-associated pathways across tissues. *Nat. Commun.* **13**(1), 4827. PMID: 35974106; doi: 10.1038/s41467-022-32552-1.

62. Scialdone A., Natarajan K.N., Saraiva L.R., Proserpio V., Teichmann S.A., Stegle O., … Buettner F. (2015). Computational assignment of cell-cycle stage from single-cell transcriptome data. *Methods* **85**, 54–61. PMID: 26142758; doi: 10.1016/j.ymeth.2015.06.021.

63. Zhou B.O., Yue R., Murphy M.M., Peyer J.G., & Morrison S.J. (2014). Leptin-receptor-expressing mesenchymal stromal cells represent the main

source of bone formed by adult bone marrow. *Cell Stem Cell* **15**(2), 154–168. PMID: 24953181; doi: 10.1016/j.stem.2014.06.008.

64. Yue R., Zhou B.O., Shimada I.S., Zhao Z., & Morrison S.J. (2016). Leptin receptor promotes adipogenesis and reduces osteogenesis by regulating mesenchymal stromal cells in adult bone marrow. *Cell Stem Cell* **18**(6), 782–796. PMID: 27053299; doi: 10.1016/j.stem.2016.02.015.
65. Gao X., Murphy M.M., Peyer J.G., Ni Y., Yang M., Zhang Y., … Morrison S.J. (2023). Leptin receptor+ cells promote bone marrow innervation and regeneration by synthesizing nerve growth factor. *Nat. Cell Biol.* **25**(12), 1746–1757. PMID: 38012403; doi: 10.1038/s41556-023-01284-9.
66. Yang F., Wu R., Jiang Z., Chen J., Nan J., Su S., … Wang J. (2018). Leptin increases mitochondrial OPA1 via GSK3-mediated OMA1 ubiquitination to enhance therapeutic effects of mesenchymal stem cell transplantation. *Cell Death Dis.* **9**(5), 556. PMID: 29748581; doi: 10.1038/s41419-018-0579-9.
67. Laschober G.T., Brunauer R., Jamnig A., Fehrer C., Greiderer B., & Lepperdinger G. (2009). Leptin receptor/CD295 is upregulated on primary human mesenchymal stem cells of advancing biological age and distinctly marks the subpopulation of dying cells. *Exp. Gerontol.* **44**(1–2), 57–62. PMID: 18573328; doi: 10.1016/j.exger.2008.05.013.
68. Freire Jorge P., Goodwin M.L., Renes M.H., Nijsten M.W., & Pamenter M. (2022). Low cancer incidence in naked mole-rats may be related to their inability to express the Warburg effect. *Front. Physiol.* **13**, 859820. Retrieved from https://www.frontiersin.org/articles/10.3389/fphys.2022.859820.
69. Oka K., Fujioka S., Kawamura Y., Komohara Y., Chujo T., Sekiguchi K., … Miura K. (2022). Resistance to chemical carcinogenesis induction via a dampened inflammatory response in naked mole-rats. *Commun. Biol.* **5**(1), 287. PMID: 35354912; doi: 10.1038/s42003-022-03241-y.
70. Wlaschek M., Singh K., Maity P., & Scharffetter-Kochanek K. (2023). The skin of the naked mole-rat and its resilience against aging and cancer. *Mech. Ageing Dev.* **216**, 111887. PMID: 37993056; doi: 10.1016/j.mad.2023.111887.
71. Wong H.-S., Freeman D.A., & Zhang Y. (2022). Not just a cousin of the naked mole-rat: Damaraland mole-rats offer unique insights into biomedicine. *Comp. Biochem. Physiol. B Biochem. Mol. Biol.* **262**, 110772. PMID: 35710053; doi: 10.1016/j.cbpb.2022.110772.
72. Gorbunova V., Hine C., Tian X., Ablaeva J., Gudkov A.V., Nevo E., & Seluanov A. (2012). Cancer resistance in the blind mole rat is mediated by concerted necrotic cell death mechanism. *Proc. Natl. Acad. Sci. U. S. A.* **109**(47), 19392–19396. PMID: 23129611; doi: 10.1073/pnas.1217211109.
73. Liang S., Mele J., Wu Y., Buffenstein R., & Hornsby P.J. (2010). Resistance to experimental tumorigenesis in cells of a long-lived mammal, the naked mole-rat (heterocephalus glaber). *Aging Cell* **9**, 626–635. PMID: 20550519; doi: 10.1111/j.1474-9726.2010.00588.x.
74. Seluanov A., Gladyshev V.N., Vijg J., & Gorbunova V. (2018). Mechanisms of cancer resistance in long-lived mammals. *Nat. Rev. Cancer* **18**, 433–441. PMID: 29622806; doi: 10.1038/s41568-018-0004-9.
75. Seluanov A., Chen Z., Hine C., Sasahara T.H.C., Ribeiro A.A.C.M., Catania K.C., … Gorbunova V. (2007). Telomerase activity coevolves with body mass not lifespan. *Aging Cell* **6**(1), 45–52. PMID: 17173545; doi: 10.1111/j.1474-9726.2006.00262.x.
76. Zavala G., Prieto C.P., Villanueva A.A., & Palma V. (2017). Sonic hedgehog (SHH) signaling improves the angiogenic potential of Wharton's jelly-derived mesenchymal stem cells (WJ-MSC). *Stem Cell Res. Ther.* **8**(1), 203. PMID: 28962669; doi: 10.1186/s13287-017-0653-8.
77. Feng M., Liu W., & Qiu Y. (2021). Sonic hedgehog induces mesenchymal stromal cell senescence-associated secretory phenotype and chondrocyte apoptosis in human osteoarthritic cartilage. *Front. Cell Dev. Biol.* **9**, 716610. PMID: 34646822; doi: 10.3389/fcell.2021.716610.
78. Emmrich S., Trapp A., Seluanov A., & Gorbunova V. (2019). An abundant myeloid progenitor shapes neonatal hematopoiesis of naked mole-rats. *bioRXiv*. doi: 10.1101/2021.08.01.454658.
79. Simic P., Zainabadi K., Bell E., Sykes D.B., Saez B., Lotinun S., … Guarente L. (2013). SIRT1 regulates differentiation of mesenchymal stem cells by deacetylating β-catenin. *EMBO Mol. Med.* **5**, 430–440. PMID: 23364955; doi: 10.1002/emmm.201201606.
80. Yuan H.-F., Zhai C., Yan X.-L., Zhao D.-D., Wang J.-X., Zeng Q., … Pei X.-T. (2012). SIRT1 is required for long-term growth of human mesenchymal stem cells. *J. Mol. Med.* **90**(4), 389–400. PMID: 22038097; doi: 10.1007/s00109-011-0825-4.
81. Pi C., Yang Y., Sun Y., Wang H., Sun H., Ma M., … He X. (2019). Nicotinamide phosphoribosyltransferase postpones rat bone marrow mesenchymal stem cell senescence by mediating NAD+–Sirt1 signaling. *Aging* **11**(11), 3505–3522. PMID: 31175267; doi: 10.18632/aging.101993.
82. Jing E., Gesta S., & Kahn C.R. (2007). SIRT2 regulates adipocyte differentiation through FoxO1 acetylation/deacetylation. *Cell Metab.* **6**(2), 105–114. PMID: 17681146; doi: 10.1016/j.cmet.2007.07.003.
83. Pan H., Guan D., Liu X., Li J., Wang L., Wu J., … Liu G.-H. (2016). SIRT6 safeguards human mesenchymal stem cells from oxidative stress by coactivating NRF2. *Cell Res.* **26**(2), 190–205. PMID: 26768768; doi: 10.1038/cr.2016.4.